Summer Greenland Blocking in reanalysis and in SEAS5.1 seasonal forecasts: robust trend or natural variability?

Johanna Beckmann[1,2,], Giorgia Di Capua[2,], Paolo Davini[3]

[1]School of Earth, Atmosphere and Environment, and ARC Special Research Initiative for Securing Antarctica's Environmental Future, Monash University, Clayton, Kulin Nations, Australia.
[2]Earth System Analysis, Potsdam Institute for Climate Impact Research, Member of the Leibniz Association, Potsdam, Germany
[3]Consiglio Nazionale delle Ricerche, Istituto di Scienze dell'Atmosfera e del Clima, Torino, Italy

 shared first authorship

Correspondence to: Giorgia Di Capua (dicapua@pik-potsdam.de)

Abstract. Given its impact on enhanced melting of the Greenland ice sheet, it is crucial to assess changes in frequency and characteristics of summer Greenland blocking. Indeed, the occurrence of such atmospheric patterns has seen a marked increase in recent decades. However, the observed trend is not captured by any simulation from state-of-the-art global climate models. It is therefore paramount to determine whether the lack of trend is caused by a misrepresentation of key physical mechanisms in climate models or whether such trend is mainly attributable to decadal variability, or both. Here we investigate Greenland blocking characteristics in reanalysis (ERA5) and ECMWF seasonal forecasts (SEAS5.1), showing that about 10% of the 1000 permutations of SEAS5.1 runs can simulate a 43-year trend equal or larger to the ERA5 one: this suggests that the initialization and the higher model resolution contribute to a more realistic representation of the blocking dynamics than in freely-evolving climate model runs. To further investigate these aspects, we apply the Peter and Clark momentary conditional independence (PCMCI) algorithm to assess monthly causal pathways. Results show that while the relationship among Arctic temperature, snow cover, Atlantic multidecadal variability and Greenland blocking is consistent both in ERA5 and SEAS5.1, the effect of early snow melt over North America on Greenland blocking is mostly absent in SEAS5.1. Therefore, while it is possible that the observed trend is due to internal decadal variability, the misrepresentation of the snow cover processes may explain the difficulty that SEAS5.1 has in reproducing the observed trend. This deficit in representing the snow impact on the atmospheric circulation might also be the culprit of the missing trend in climate models, raising the question whether long-term projections underestimate a future increase in Greenland blocking and ice sheet melt.

1 Introduction

Atmospheric blocking over Greenland can be defined by the occurrence of a persistent anticyclone in the mid-troposphere in proximity to Greenland (Hanna et al. 2016). More precisely, it is a large-scale atmospheric high-pressure low-vorticity system associated with the negative phase of the North Atlantic Oscillation (Woollings and Hoskins, 2008).

Despite being less studied than its winter counterpart, summer Greenland blocking presents characteristics that can severely impact the Greenland ice sheet which has recently put it at the centre of the attention of the scientific community (Hanna et al., 2018; McLeod and Mote, 2016; Tedesco and Fettweis, 2020, Wang and Luo, 2022). Due to its anticyclonic structure, during periods of strong Greenland blocking southerly advection of warm air on the western side of Greenland favours enhanced melting (McLeod and Mote, 2016). Indeed, blocking has been associated with extreme melt years in recent years (Tedesco et al., 2011, Nghiem et al., 2012, Tedesco and Fettweis, 2020). Moreover, modelling studies suggest that if these extreme melting years increase in frequency in the future, the contribution to sea level rise from the Greenland Ice Sheet could increase by 20% by the end of the 23rd century (Beckmann and Winkelmann, 2023).

Most importantly, evidence is accumulating in recent years showing that the frequency of occurrence of summer Greenland blocking has been increasing in the last two decades (Hanna et al., 2018; Wachowicz et al., 2021). This is most relevant considering that state-of-the-art climate models seem to lack agreement with the observed positive blocking trends for summer Greenland blocking, questioning whether projected future changes for blocking – and indirectly for ice sheet melting - are reliable (Davini and D'Andrea, 2020; Delhasse et al., 2020; Maddison et al., 2024; Masato et al., 2013).

Despite being weaker in summer months, Arctic amplification (AA), i.e. the phenomenon that sees the Arctic region warming at a pace two-to-four times faster than the rest of the Northern Hemisphere (Cohen et al., 2014; Davy et al., 2018; Previdi et al., 2021; Serreze et al., 2009) has been suggested to influence circulation patterns in the northern mid-latitudes and possibly influence blocking (Cohen et al., 2014; Francis and Skific, 2015; Nakamura et al., 2016): enhanced Arctic warming can affect weather patterns, leading to weaker storm tracks, shifts in the position of the jet stream and favouring the amplification and persistence of Rossby waves (Coumou et al., 2018).

However, a clear understanding of the underlying mechanisms leading to the observed Greenland blocking increase is not yet available. Preece et al. (2023) proposed a mechanism which connects reduced snow cover in late spring over the North American continent with the formation of a Rossby wave pattern, which in turn enhances blocking over Greenland in the following summer. However, the large interannual variability of the region, which is often described as a red noise process (Feldstein, 2000) and can present years of extremely high blocking frequency followed by years where almost no blocking is observed, still questions the real presence of a long-term trend (Davini et al., 2021; Gollan et al., 2015). For example, in recent years the trend of Greenland blocking has weakened (Preece et al., 2023) leaving open the possibility that the increase is a consequence of natural variability. In this direction, natural climate variability modes, such as the Atlantic Multidecadal Variability (AMV), may impact large scale circulation patterns in the North Atlantic, and the local jet stream dynamics, thus

---

67 indirectly affecting blocking onset and maintenance, and further complicating the scenario (Häkkinen et al., 2011; Luu et al.,
68 2024).
69 Beyond high- and mid-latitude drivers, tropical sea surface temperatures and convection can affect summer climate over
70 Greenland and the Arctic, including Rossby wave trains that enhance sea ice melt (Baxter et al., 2019). Model experiments
71 forced with tropical sea surface temperatures show that anomalies in mid-to-upper-tropospheric anticyclonic wind may explain
72 half of the observed Greenland surface warming and ice loss acceleration over the last three decades (Topál et al., 2022).
73 Another element which further tangles up the Greenland blocking puzzle is related to its representation in climate models.
74 While modelling blocking has always been a challenge for both numerical weather prediction models and global climate
75 models, significant improvements have been achieved in the last 25 years (Davini and D'Andrea, 2016, 2020). However,
76 evidence is emerging that none of the Coupled Model Intercomparison Project - Phase 5 (CMIP5) and Phase 6 (CMIP6)
77 models, among the hundreds of ensemble members available, is capable of replicating the observed increasing trend of summer
78 Greenland blocking, and neither project a significant increase through 2100 (Delhasse et al., 2020; Luu et al., 2024; Maddison
79 et al., 2024). Moreover, CMIP6 models also fail to capture the magnitude of the melting events, such as the one observed in
80 summer 2019, hinting at a potential underestimation of ice sheet mass loss over Greenland (Delhasse et al., 2020).
81 Such lack of trends questions the capability of CMIP6 models to capture features such as the Arctic amplification and
82 significantly weakens the reliability of their climate predictions. In this context, identifying the atmospheric and surface drivers
83 of Greenland blocking variability, both in observations and general circulation models, can help assess which physical
84 mechanisms govern the variability of Greenland blocking and which of the identified mechanisms can be confidently
85 reproduced by climate models.
86 Causal discovery can help identify causal relationships in a set of different climate and atmospheric variables (Di Capua et al.,
87 2020b; McGraw and Barnes, 2020; Runge et al., 2019a) and provides a tool to validate model performance in reproducing
88 atmospheric causal pathways (Di Capua et al., 2023; Nowack et al., 2020). The Peter and Clark momentary conditional
89 independence (PCMCI) algorithm is a causal discovery tool that helps identify true causal relationships from spurious
90 correlation values (Runge, 2018; Runge et al., 2019a, b). With respect to other causal discovery tools, such as Granger
91 causality, PCMCI allows us to assess the possible effect of a (set of) third variable(s). However, when compared to other causal
92 discovery techniques, such as the Liang–Kleeman information flow, PCMCI yields very compatible results, thus providing a
93 robust tool for the identification of causal relationships (Docquier et al., 2024). PCMCI has found several applications in the
94 field of climate and atmospheric sciences, ranging from the identification of tropical – extratropical teleconnections in
95 observations and forecasting models (Di Capua et al., 2020a, 2023) to stratospheric pathways leading to sudden stratospheric
96 warming events (Kretschmer et al., 2016, 2018a), climatological variability (Di Capua et al., 2019; Lehmann et al., 2020;
97 Pfleiderer et al., 2020), and much more (Tian et al. 2024, Di Capua et al., 2024).
98 In the current work, we investigated the Greenland blocking representation in state-of-the-art multi-member high-resolution
99 monthly-initialized seasonal forecast system, namely the European Centre for Medium-range Weather Forecasts (ECMWF)
100 SEAS5.1 forecast system, to understand to what extent, initialization characteristics and high resolution could help in capturing

105 the observed summer Greenland blocking trend. Robustness of the blocking climatology of SEAS5.1 has been already assessed
106 (Davini et al., 2021), so that this will help us disentangling the role of natural variability from that of anthropogenic climate
107 change in affecting the variability and trends of Greenland blocking, hence helping to resolve a piece of the complex puzzle
108 of Greenland blocking trend. The remainder of this manuscript is organized as follows: we first describe the data and method
109 used (Sect. 2), then present the results obtained (Sect. 3) and finally discuss the results (Sect. 4).

110 **2 Data and Methods**

111 **2.1 Data**

112 We analyse daily atmospheric fields and snow cover fields during the boreal summer period (June to August, JJA) using
113 gridded data (0.25°x0.25° spatially regridded to 1°x1°) for the period 1940-2023 from the ERA5 reanalysis dataset (Hersbach
114 et al., 2020) and for the period 1981-2023 from the SEAS5.1 seasonal forecast dataset (Johnson et al., 2019), both provided
115 by the European Centre for Medium-range Weather Forecasts (ECMWF). Specifically, we consider daily (temporally averaged
116 to obtain monthly samples) geopotential height at 500 hPa (Z500), 2m temperature (T2m), snow cover (Snow), sea surface
117 temperature (SST) and mean sea level pressure (MSLP). Snow is obtained from snow density and snow depth fields (see Text
118 S1 in the Supplementary Material). For ERA5, we use the entire 1940-2023 period (referred in the text as ERA5-40) to assess
119 long term trends. However, for the most part of the analysis we use the 1981-2023 period (ERA5-81), to allow a direct
120 comparison with the SEAS5.1 dataset. To focus on dynamic linkages, for each of the three-month time steps considered in

> Deleted: monthly

121 each JJA season, the trend over the 43 years for ERA5-81 (or 84 years for ERA5-40) is removed and anomalies around zero
122 are calculated, thus removing both the trend and seasonal cycle. Note that data are not detrended when historical trends are
123 analysed.
124 SEAS5.1 initialized on March 1 (SEAS5.1-03), May 1 (SEAS5.1-05) and June 1 (SEAS5.1-06) have been used. Although
125 SEAS5.1 provides 51 ensemble members, 25 ensemble members each year are publicly available through the Copernicus
126 Climate Data Store, thus a total of 25x43 (1075) model years. SEAS5.1 data are extracted from the initialization date until
127 October 1, thus a total of seven, five and four months are available for SEAS5.1-03, SEAS5.1-05 and SEAS5.1-06 respectively.
128 As for ERA5, also for SEAS5.1 data, we provide monthly averages, remove the trend over the 1981-2023 period and calculate
129 anomalies centred around zero.

130 **2.2 Greenland blocking indices**

131 Atmospheric blocking can be detected in several ways which can lead to apparently contradictory results, strongly affected by
132 the index chosen for its identification (Woollings et al., 2018). As for other blocking regions, multiple approaches have been
133 proposed to identify the blocking anomaly over Greenland (Hanna et al. 2016, 2018; Wachowicz et al., 2020). In the current
134 work, we adopt an atmospheric blocking index which follows the original definition by Tibaldi and Molteni (1990) but
135 extended to a 2-D field following Scherrer et al. (2006) and Davini et al (2012a). This is an index based on the reversal of the

137   meridional gradient of the Z500 field: in contrast to other indices based on anomaly measures, it targets the presence of easterly

138   winds to the south of the blocked grid point, providing a dynamical relevant definition of the phenomenon. To define the index,

139   two meridional geopotential height gradients at southern (GHGS) and northern (GHGN) latitudes are defined:

140    $GHGS(\lambda_0, \varphi_0) = \frac{Z500(\lambda_0, \varphi_0) - Z500(\lambda_0, \varphi_S)}{\varphi_0 - \varphi_S}$,   (1)

141    $GHGN(\lambda_0, \varphi_0) = \frac{Z500(\lambda_0, \varphi_N) - Z500(\lambda_0, \varphi_0)}{\varphi_N - \varphi_0}$,   (2)

142   where φ_0 ranges from 30° to 75°N and λ_0 ranges from 0° to 360°E. $\varphi_N = \varphi_0 + 15$ and $\varphi_S = \varphi_0 - 15$, such that the gradients

143   are always calculated 15° North and 15° South of φ_0. The GHGS index defines where the reversal is happening, and it is the

144   key element for the identification of blocking. GHGN ensures the presence of westerly winds northward to the blocked area,

145   focusing on the presence of a high-pressure dome over the analysed region. To ensure that the blocking index is not detecting

146   a poleward migrating subtropical ridge – a condition typically occurring in summer months in Northern Hemisphere (i.e. that

147   easterly winds are not caused by trade winds), a supplementary definition from Davini et al. (2012a) is introduced, and named

148    $GHGS_2$:

149    $GHGS_2(\lambda_0, \varphi_0) = \frac{Z500(\lambda_0, \varphi_S) - Z500(\lambda_0, \varphi_{S_2})}{\varphi_S - \varphi_{S_2}}$,   (3)

150   Where $\varphi_{S_2} = \varphi_S - 15°$.

151   Consequently, at daily time scales, blocking is thus identified when:

152    $GHGS(\lambda_0, \varphi_0) > 0$,

153    $GHGN(\lambda_0, \varphi_0) < -\frac{10m}{°lat}$

154   and $GHGS_2(\lambda_0, \varphi_0) = -\frac{5m}{°lat}$

155   Blocking is thus a binary index, which can be spatially averaged over Greenland (55°W-0°, 67°N-75°N) to produce what we

156   define as the Greenland blocking index (GBI). Note that the GBI region is identified based on where a significant positive

157   trend in the 2-D blocking index is detected (Fig. 1a).

158   However, such a binary index focuses on the exceptional non-linearity of blocking itself. Given that the target of this analysis

159   is the long-term trend in the strength and shape of geopotential height over Greenland, we also introduce a continuous (non-

160   binary) index, which is obtained as the linear combination of GHGS and GHGN. Indeed, at high latitudes, GHGS$_2$ is found to

161   have a negligible role (not shown). Thus, we define the Greenland gradient index (GGI) so that $GGI = GHGS - GHGN$,

162   which is then highly correlated with GBI. GGI represents an alternative measure to standard blocking and can be physically

163   interpreted as a measure of the strength of the geopotential height anomaly. In both cases – given the limited impact that such

164 constraint has on the real pattern and frequency of blocking – we followed the approach of previous literature (Davini and
165 D'Andrea, 2020; Tibaldi and Molteni, 1990) and we do not apply any spatial or temporal constraint to the blocking index.
166 Given the wide diversity of possible blocking indices, other alternatives have been explored. The Greenland Blocking Index
167 developed by Hanna et al. (2016), hereafter the HA16 Index, has been computed to provide a sensitivity to an absolute detection
168 method (i.e. not based on gradient reversal). The HA16 Index is a punctual index defined only for Greenland, and it uses the
169 area weighted geopotential height absolute values at 500hPa in the box delimited by 60N-90N, 80W-20W.
170 Similarly, the updated gradient reversal method for high latitude blocking developed by the Tyrlis et al (2021), hereafter the
171 TY21 index, has been computed. This index, which shares with the Davini et al. (2012) method the most of its definitions,
172 loosens the criteria for GHGN asking only to be smaller than 0 for latitude north of 60N. This - according to the authors -
173 allows for a more precise detection of blocking at higher latitude more aligned with blocking detected on isentropic surfaces.

2.3 Causal discovery and causal inference

175 In the present work, we apply the Peter and Clark momentary conditional independence (PCMCI) algorithm, a causal discovery
176 tool which allows to disentangle spurious from actual *causal* relationships in a set of univariate time series. In general, (cross-
177) correlation measures are often used to determine the existence of concurrent behaviour between pairs of time series. However,
178 correlation does not imply causation, and spurious correlations can arise from common effects like (i) the presence of strong
179 auto-correlation in one (or both) time series, (ii) common drivers or (iii) indirect links. Thus, two time series may be both
180 driven by a third time series (common driver) and therefore show a significant correlation even though no real causal link is
181 present. PCMCI deals with these issues by iteratively testing for the presence of significant partial correlations (in the linear
182 framework) between pairs of time series by conditioning on a set of one (or more) further time series.
183 The PCMCI algorithm is composed of two steps, the PC-step and the MCI-step. In the PC-step, the algorithm first identifies
184 all significant lagged (up to a certain prescribed lag t_{max}) correlations among all possible combinations of time series in the set
185 of time series (actors), e.g. $P = \{A, B, C, D, F\}$. The first set of "potential parents" for each time series is identified, e.g. with
186 $t_{max} = -3$, $P_A^0 = \{A_{t=-1}, B_{t=-2}, C_{t=-1}, D_{t=-3}, D_{t=-2}\}$. Then, the algorithm tests whether the partial correlation between $A_{t=0}$ and
187 each element x_i in P_A^0 is still significant when conditioning on a combination of the remaining elements $x_j \neq x_i$ in P_A^0. The
188 partial correlation is calculated by (linearly) regressing $A_{t=0}$ and x_i on x_j, and then taking the correlation of the residuals of
189 $A_{t=0}$ and x_i. If this partial correlation is still significant, then $A_{t=0}$ and x_i, will be considered "conditionally dependent",
190 meaning that their correlation cannot be explained by the linear combination of x_j. In the PC-step, the number of conditions x_j
191 gradually increases until the number of elements in the set of potential parents P_A^n is equal or smaller than the number of
192 iterations. At the end of the PC-step, each time series in P will have its own set of potential patents, e.g. $P_A^n = \{A_{t=-1}, C_{t=-1}, D_{t=-2}\}$ and $P_B^m = \{B_{t=-2}, D_{t=-1}, A_{t=-2}, E_{t=-3}\}$.
194 In the MCI-step, the partial correlation is calculated again between all potential pairs of actors in P. However, this time the
195 partial correlation is only calculated once by conditioning on the common set of parents identified in the PC-step. E.g. if $A_{t=0}$

198 and $B_{t=-1}$ are tested, then the partial correlation will be calculated using the joint set of parents of $A_{t=0}$ and $B_{t=-1}$, the latter

199 being equal to the set of parents of $B_{t=0}$ which has been adjusted for lag -1. The actors found to be conditionally dependent in

200 the MCI-step define the set of causal parents for each time series. Finally, the significance of the detected causal links (each

201 partial correlation has its own p-value) is corrected by applying the Benjamini-Hochberg false discovery rate (FDR) (Benjamini

202 and Hochberg, 1995), which accounts for the fact that the same hypotheses are iteratively tested multiple times. The corrected

203 p-values then determine whether a link between two actors is considered "causal".

204 The causal effect is then calculated by linearly regressing each actor on its own set of causal parents. E.g., assuming that the

205 causal parents of $A_{t=0}$ are $P_A^n = \{A_{t=-1}, C_{t=-1}, D_{t=-2}\}$, then the following multilinear regression equation will be calculated:

206 $$A_{t=0} = \beta_A * A_{t=-1} + \beta_C * C_{t=-1} + \beta_D * D_{t=-2} + \xi_A \qquad\qquad (4)$$

207 Where β_i is the causal effect of each parent x_i. With standardized actors, a β_B value of 0.5 corresponds to a change of 0.5

208 standard deviation (s.d.) of $A_{t=0}$ given a change of 1 s.d. of $B_{t=-1}$ (given that all other parents remain unaltered). In this work,

209 we use the PCMCI algorithm as coded in Tigramite, version 5.2, and we use the PCMCIplus function, which allows us to

210 calculate links also at lag 0. However, lag 0 links are not "directed", which means that the direction of causality is not

211 determined. The Tigramite package is publicly available and can be found at this link https://github.com/jakobrunge/tigramite.

212 The causal relationships obtained with PCMCI are then plotted in a causal effect network (CEN). In a CEN, each actor is

213 represented by a node in the network, while lagged causal relationships are represented by directed arrows, showing the

214 direction of causality. The colour of the arrows (nodes) shows the strength of the causal effect, the β value (auto β value), while

215 the numbers on the arrows show the lag at which the causal link is detected. Finally, the causal effect can also be calculated

216 by applying the concept of causal inference, rather than causal discovery. When causal inference is applied, the causal links

217 are determined a priori (generally based on expert-knowledge of the analysed physical system) and then the causal effect is

218 calculated following the same multi-linear regression model described earlier in Eq. (4). A detailed description of the Tigramite

219 functions and parameters used can be found in Text S2 in the Supplementary Material.

220 Here, linear correlation analysis and probability-trend estimation were conducted for all datasets mentioned. The correlation

221 and causal inference analyses were performed for both SEAS5.1-03 and SEAS5.1-05, except for CENs. For causal discovery,

222 only SEAS5.1-03 was used, as the absence of March and April data in SEAS5.1-05 violates PCMCI algorithm requirements.

223 Therefore, we mainly present results for SEAS5.1-03 in the main manuscript, while SEAS5.1-05 is available in the

224 Supplementary Material.

225 **2.4 Bootstrapping and significance**

226 To ensure statistical significance in the seasonal forecast data (SEAS5.1 initialized in March, May, and June), we employed

227 bootstrapping. We resampled the original set of 25 ensemble members x 43 years, creating 10,000 new samples by randomly

228 selecting one of the 25 ensemble members for each year along the timeseries from 1981 to 2023. This resampled distribution

229 of 10,000 timeseries is illustrated in various figures. When a single value for SEAS5.1 is mentioned, it refers to the median of

Deleted:) ,

231 the bootstrapped distribution. For example, the correlation between two indices in SEAS5.1 is determined by calculating the

232 correlation values for all 10,000 timeseries and then taking the median of these values.

3 Results

3.1 Greenland blocking indices and trends

235 Greenland blocking in the summer season has increased its frequency in recent decades. Figure 1a and 1b show the grid-point

236 blocking frequency trends defined by the JJA seasonal averaged blocking index for ERA5 reanalysis for two different time

237 windows. However, notable differences emerge when focusing on different time windows: while in ERA5-40 the blocking

238 trend is positive in most of the Northern Hemisphere (Fig. 1a), the linear trend shows much larger spatial variability when

239 ERA5-81 is considered (Fig 1b), showing decrease in western Europe and western North America. Still, over the Greenland

240 Blocking region, highlighted by the red box in both panels, trends remain positive irrespective of the period considered.

241 The difference between the two trends may be related to the large interannual variability which characterizes blocking.

242 Blocking can easily achieve a frequency of 20% in certain summers and then show an almost negligible frequency in the

243 following year. This can be also seen in Figure 1c, where both the GBI (blue) and GGI (red) indices are reported, and the

244 year-to-year variability emerges evidently. A significant positive trend is observed in both cases (trends are significant at 99%

245 confidence level for both indices with a Mann-Kendall test). However, recent years are characterized by a reduction of blocking

246 from 2015 onward, which weakens the magnitude and the significance of the trend (Fig. S1 in the Supplementary Material).

247 It is important to notice that the seasonal averaged GGI and GBI indices are also highly correlated, showing a Pearson

248 correlation coefficient of $r = 0.8$. From a statistical point of view, this implies that the two indices are very similar and in the

249 rest of the manuscript we will employ GGI to perform the PCMCI analysis, which works best with non-binary indices.

250 Similar results can be obtained when using different blocking indices, as the HA16 and TY21 indices. Despite minor

251 differences inherently associated with their definitions, both indices display the same qualitative trends as seen in Fig. 1c (Fig.

252 S2-3 in the Supplementary Material).

253
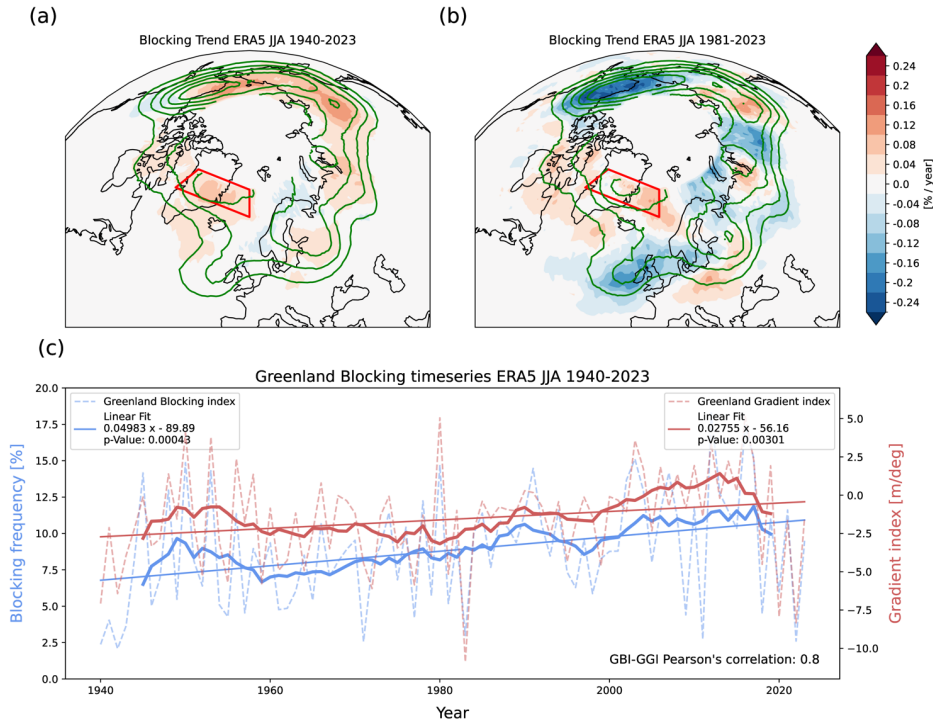
Figure 1: Greenland blocking index observed trends. Panel (a) shows blocking trend (shading) and blocking climatology (green contours in boreal summer (JJA) over the Northern Hemisphere for ERA5-40. Contours are drawn every 3% blocked days. Panel (b): same as for Panel (a) but for ERA5-81. Panel (c) shows JJA Greenland Blocking Index (blue) and Greenland Gradient Index (red), measured as the averaged over the red box shown in panel (a) for ERA5-81. Dashed lines show the season average, bold lines the 10-year running mean and the thin solid lines the linear trend. Values for the trend and their *p*-values (estimated with a Mann-Kendall test) are shown in the legend for both indices.
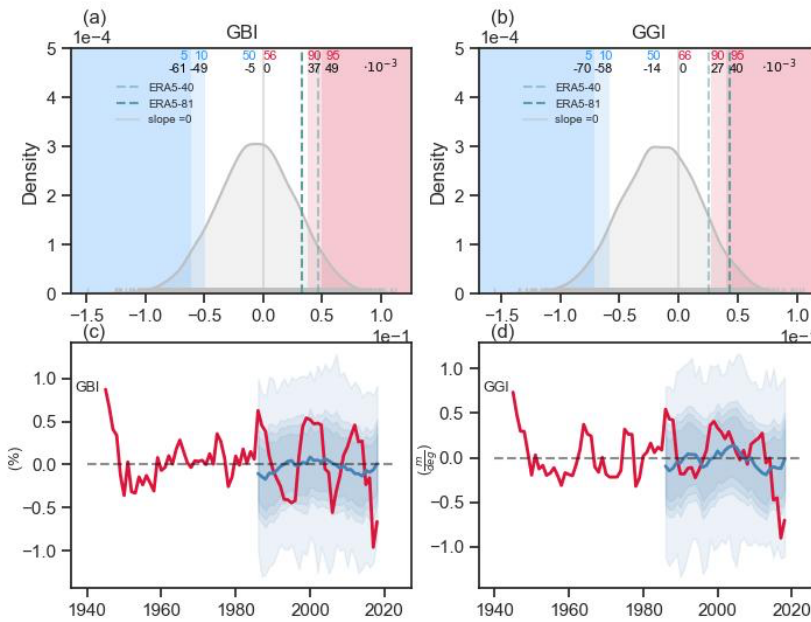
260
261 **Figure 2: Greenland blocking and Greenland Gradient index trends in SEAS5.1-03 and ERA5.** Panel (a) shows the Probability density
262 function of JJA trends in GBI for the 10^4 different member permutations. Panel (b): same as for panel (a) but for the GGI index. Shaded
263 vertical lines show values 5th,10th, 90th and 95th percentiles. Percentiles are shown in blue (5th,10th, 50th) and red (90th and 95th) with the
264 corresponding trend values in black below. Percentile of the distribution of a slope of 0 is also given in red and indicated with the grey
265 vertical line. Green dashed verticals indicate linear slope of ERA5-40 (light green) and ERA5-81 (solid green). Panel (c) shows the 11-year
266 moving window trend of ERA5 (red) and the SEAS5.1-03 trend distribution (blue shadings) for the GBI. Panel (d) same as for panel (c) but
267 for the GGI index. The dark blue line indicates the median 11-year running mean of the SEAS5.1-03 distribution.

268

269 Observed trends in GBI and GGI are shown in detail in Fig. 2. To compare the ERA5 trend with SEAS5.1-03 trends, we

270 calculate a probability density function (PDF) of the 10^4 trends derived from our bootstrapped SEAS5.1-03 ensemble members

271 (see Methods Section 2.4). In contrast to ERA5, the median values of the SEAS5.1-03 PDFs indicate negative trends for both

272 GGI and GBI (Figs. 2a and 2b respectively). The ERA5-81 trend falls right below the 90th percentile for GBI (Fig. 2a) and

273 between the 90th and the 95th percentiles for GGI (Fig. 2b). This suggests that albeit SEAS5.1-03 can reproduce the observed

274 trends with certain specific combinations of ensemble members, the probability of doing so is relatively low (~5-10%). Using

275 later initialization dates (SEAS5.1-05 and SEAS5.1-06) does not increase the likelihood of matching the observed trends (see
276 Fig. S4 in the Supplementary Material). We provide the same analysis using the GHGS and GHGN components of the
277 Greenland Blocking index (Fig. S5 in the Supplementary Material) and show that the probability of reproducing the observed
278 trend is slightly higher for GHGN, while it is very low for GHGS (below 2.5%), indicating that GHGS may be the primary
279 source of the low agreement between ERA5 and SEAS5.1 trends. We also check the trends obtained with the HA16 index,
280 which shows qualitatively similar results (see Fig. S6 in the Supplementary Material).

281 To investigate the multidecadal variability of the blocking trends, we run an 11-year moving window trend on the ERA5 and
282 SEAS5.1 timeseries (Figs. 2c and 2d). SEAS5.1 trends are shown both as the ensemble mean trend (blue solid line in Fig. 2c-
283 d), or as the distribution of trends obtained from each of the 10^4 realizations (blue shading in Fig. 2c-d). The timeseries of
284 ERA5 reveals that the short-term blocking trend (for both GBI and GGI) fluctuates between positive and negative values,
285 indicating a strong influence from climate variability on decadal timescale. Particularly in recent years, the moving window
286 trend shows remarkable negative trends, which explains the loss of significance for the GBI observed for the ERA5-81 trend
287 (Fig. S1). The ERA5 moving window trend lies in the ensemble of the bootstrapped SEAS5.1 ensemble, where the median
288 SEAS5.1 trend shows a switching of the sign as well but not always aligned with ERA5.

290 Next, we check the relationship between GGI and surface temperatures over the extended North Atlantic sector (Figs. 3a-b),
291 to quantify the relationship between high GGI indices and positive temperature anomalies over the Greenland ice sheet in both
292 reanalysis and seasonal forecast. We calculate composites of T2m and Z500 fields during days for which GGI values are
293 greater than their JJA s.d. (GGI > 1 s.d.) for both ERA5-81 (Fig. 3a) and SEAS5.1-03 (Fig. 3b) datasets. Z500 composites for
294 ERA5 show the expected ridge centred over eastern Greenland, which is paired with a trough to the south, centred west of the
295 British Isles (Fig. 3a). This north-south dipole pattern is also present with a similar shape, location and strength of the Z500
296 anomalies in the SEAS5.1-03 composite (Fig. 3b). Positive T2m anomalies are shown over Greenland for both ERA5 and
297 SEAS5.1-03, reaching values of +2.5K while over the Arctic Ocean and the North Atlantic weak negative anomalies are shown
298 (-0.5K, shading in Figs. 3a-b). The difference between SEAS5.1-03 and ERA5 composites for both T2m and Z500 shows a
299 tendency of the model to have higher Z500 anomalies over Greenland and the North Atlantic and higher T2m anomalies over
300 Greenland and Northern Canada with respect to ERA5 (Figs. 3c-d).
301 The PDF showing the distribution of the GGI index is shown in Fig. 3e for ERA5-81 and Fig. 3f for SEAS5.1-03 and provides
302 a measure of the daily variability of the Z500 field over Greenland in summer. The JJA GGI mean value is -1.52 m for ERA5-
303 81 and -1.39 m for SEAS5.1-03, while the s.d. values are 10.1 m and 11.8 m respectively. Thus, the variance in SEAS5.1-03
304 is slightly overestimated with respect to ERA5-81. Note that GGI values are detrended and the anomalies are centred around
305 zero (as described in Section 2.1).
306

307 High pressure systems over Greenland are associated with high temperature anomalies both in SEAS5.1 and ERA5 (Fig. 3a-

308 b). Temperature over Greenland is then calculated by spatially averaging T2m values over the box 67-81°N, 25-55°W and the

309 corresponding index is named T2m-Greenland (T2m-G). The JJA climatological PDFs for T2m-G for ERA5 and SEAS5.1-

310 03 are shown in Figs. 3g and 3h respectively (orange shading in Figs. 3g-h). T2m-Greenland for SEAS5.1 has a comparable

311 mean value and slightly larger standard deviation than ERA5.

312 The effect of GGI on T2m is then quantified by calculating the T2m-G PDFs sub-selecting only days for which GGI > 1 s.d.

313 (shown are red lines in Figs. 3g-h). For ERA5-81, the T2m-G PDF strongly shifts towards higher T2m values for GGI > 1 s.d.,

314 with 85% of the values falling above the 50th quantile and 28% of the data exceed the climatological 90th quantile, thus showing

315 a 3-fold increase in the probability of extreme heat (Fig. 3g). Similarly, the SEAS5.1-03 T2m-G PDF for days where GGI > 1

316 s.d. also shows a strong shift towards higher T2m values, with 88% of the data falling above the 50th climatological quantile

317 and 35% of the data exceed the 90th climatological quantile, consistently showing a 3-fold increase in extreme T2m-G values

318 (Fig. 3h). Hence, high GGI values are generally related to higher than average T2m-G values both in ERA5-81 and SEAS5.1-

319 03, showing a good linkage between geopotential height anomalies and temperature anomalies in the seasonal forecast system.

320 However, the relationship to extreme T2m-G values is more marked in SEAS5.1-03.

321 The same Figures but for GGI SEAS5.1-05, for SEAS5.1-03 GHGS and GHGN, as well as for the HA16 index show consistent

322 results, even though for positive GHGN values the sign of the Z500 and T2m anomalies is inverted (see Supplementary

323 Material, from S7 to S10).

324
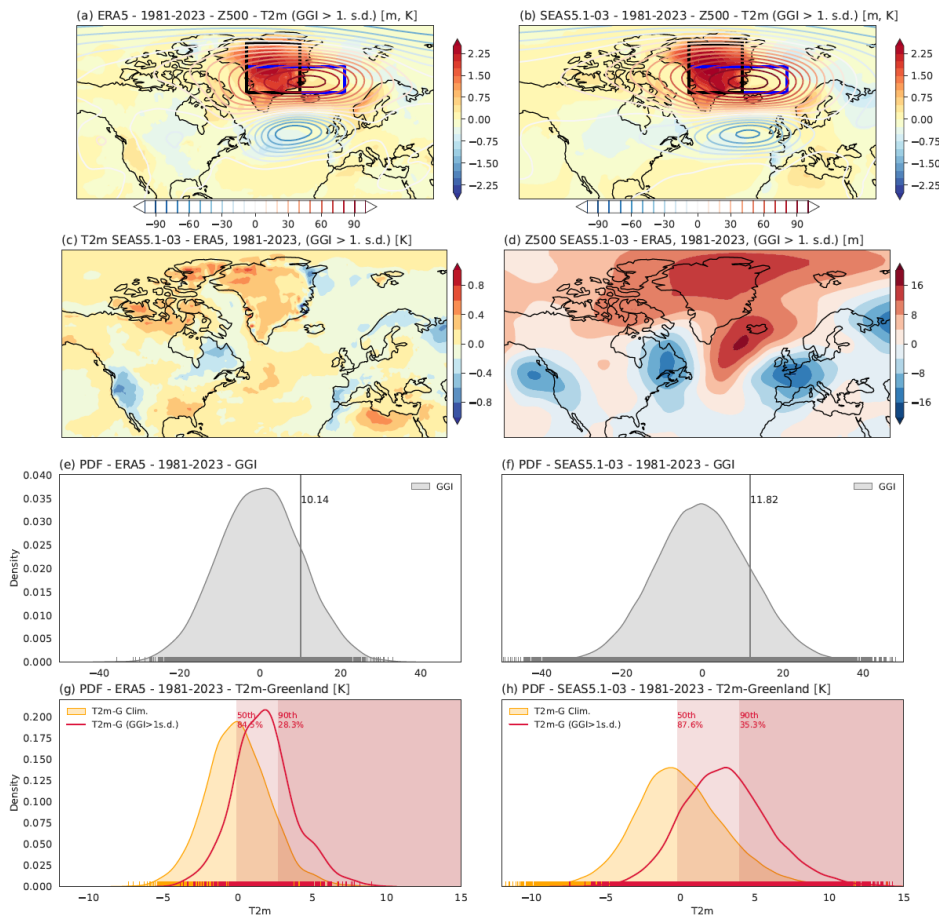
Figure 3. GBI and extreme temperatures over Greenland. Panel (a): composite of JJA Z500 (contours) and T2m (shaded) anomalies for (daily) time steps with GGI > 1 s.d. for ERA5-81. Panel (b): Same as panel (a) but for the SEAS5.1-03 dataset (25 ensemble members each year). Panel (c): difference between the SEAS5.1-03 and the ERA5 T2m composites shown in Panels (a)-(b). Panel (d): Same as for Panel (c) but for the Z500 field. Panel (e): probability density function (PDF) for the Greenland gradient index (GGI) daily climatology for ERA5-81. Panel (f): Same as for Panel (e) but for SEAS5.1-03 dataset. Panel (g): PDF for the T2m-Greenland (T2m-G) daily climatology (orange) and sub-selected days with GGI > 1 s.d. (red) for ERA5-81. Red shading in the plot highlights the position of the climatological 50th and 90th percentiles, while the numbers below the percentiles show the percentage of T2m-G which is above the climatological percentile in the sub-selected PDF. Panel (h): Same as for Panel (g) but for SEAS5.1-03.

3.2 Potential drivers of Greenland blocking at monthly time scales

We identify four potential drivers for GGI variability based on hypothesized mechanisms described in Section 1. These potential drivers are: (i) T2m over the Arctic circle (T2m-Arctic, an indicator for Arctic warming), (ii) snow cover over northern North America (Snow-NAm), (iii) MSLP over the eastern North America (MSLP-NAm, following the mechanism identified by Preece et al 2023) and (iv) the Atlantic Multidecadal Variability (AMV) index. The spatial domain and acronym of each index is reported in Table 1 and resulting analysis is presented in Figure 4.

Figures 4a,e show the composites of T2m fields over months where the T2m-Arctic index is above 1 s.d. (T2m-Arctic > 1 s.d.) for ERA5-81 and SEAS5.1-03 respectively. As expected, high surface temperature anomalies up to 2°C are seen over the polar cap (latitude > 60°N) over land, while over the Arctic Ocean weak negative anomalies are detected. This result confirms the tendency of high-latitude land to warm up more strongly in summer, compared to the Arctic Ocean (Di Capua et al., 2021). Over mid-latitude and tropical land-ocean surfaces, T2m anomalies tend to be positive both in ERA5-81 and SEAS5.1-03. However, in SEAS5.1-03 T2m anomalies are much weaker outside the Arctic circle (Fig. 4e), while in ERA5 strong warming is also detected over Europe, western Russia, the Middle East, southwestern United States and mid-latitude North Pacific (Fig. 4e). This discrepancy between ERA5 and SEAS5.1-03 may be explained by the different size of the two sub-samples: while ERA5-81 contains a total of 3*43 = 129 summer months, SEAS5.1-03 contains 25 times more. Since 1940, T2m-Arctic has shown a significant positive trend that has doubled in the time frame from 1981-2023 (Figure S11 in the Supplementary Material). The 11-year moving window trend (Fig. 4i) shows that T2m-Arctic fluctuates between positive and negative values since 1940 but has stayed positive since around 2000. The majority of the bootstrapped SEAS5.1-03 experiences this continued positive trend as well indicated by the blue-shaded ensemble distribution in Fig. 4i and the SEAS5.1-03 median values in thick blue, showing that the polar cap warming is well captured by the model.

Index	Acronym	Spatial domain
Greenland blocking index	**GBI**	55°W-0°, 67°N-75°N
Greenland gradient index	**GGI**	55°W-0°, 67°N-75°N
Geopotential height gradient South	**GHGS**	55°W-0°, 67°N-75°N
Geopotential height gradient North	**GHGN**	55°W-0°, 67°N-75°N
Atlantic multidecadal variability	**AMV**	80°W-0°, 0°-60°N
Snow cover over North America	**Snow-NAm**	70°-135°W, 40°-75°N
Mean sea level pressure over North America	**MSLP-NAm**	70°-105°E, 30°-50°N
Arctic 2m temperature	**T2m-Arctic**	180°W-180°E, 60°-90°N

Table1. Summary of indices with their corresponding acronyms and spatial domains.

358 Composites for Snow over North America during months with Snow-NAm < 1 s.d. (May only) are shown in Fig. 4b,f for

359 ERA5-81 and SEAS5.1-03 respectively. ERA5-81 shows lower than average Snow anomalies over Alaska, at the border

360 between the United States and Canada, and in Siberia (Fig. 4b), while SEAS5.1-03 only shows negative Snow anomalies over

361 North America (Fig. 4f). Since 1960, the 11-year moving window trend of Snow (Fig. 4j) has generally shown negative values,

362 with only brief and minor episodes of positive values. In recent years, there has been a positive trend in the ERA5 Snow data;

363 however, the overall snow cover remains below the 1940-2023 mean (Fig. S11 in the Supplementary Material). Meanwhile,

364 the SEAS5.1-03 ensemble exhibits significant fluctuations between positive and negative 11-year moving window trends (Fig.

365 4j), suggesting that snow cover may not be accurately captured in SEAS5.1.

366 Composites for MSLP fields during months with MSLP-NAm < 1 s.d. are shown in Figs. 4c and 4g for ERA5-81 and SEAS5.1-

367 03 respectively. Months with low MSLP-NAm are associated with low MSLP anomalies over North America, the mid-latitude

368 North Atlantic both for ERA5-81 and SEAS5.1-03. High MSLP anomalies are shown over the Arctic circle and Greenland

369 (Figs. 4c-g). The 11-year moving window trend of MSLP-NAm has shown strong fluctuations between positive and negative

370 trends throughout the entire period from 1940 to 2023 (Fig. 4k). These fluctuations are well captured by the bootstrapped

371 SEAS5.1-03 ensemble since 1981. Over the whole timeseries, we can see a statistically significant negative trend in MSLP-

372 Nam for ERA5, with a doubling of the negative slope since 1981 (Fig. S11 in the Supplementary Material).

373 Finally, composites for SST anomalies during months with AMV > 1 s.d. are shown in Fig. 4d,h for ERA5-81 and SEAS5.1-

374 03 respectively (the AMV is calculated following Zhang et al (2019), see Text S3 in Supplementary). Positive SST anomalies

375 are found over high-latitude North Atlantic, west of the European and African coasts and over the tropical North Atlantic,

376 while cold anomalies are shown over mid-latitude eastern North Atlantic (Figs. 4d,h). Cold anomalies are also seen over the

377 western North Pacific for both ERA5-81 and SEAS5.1-03, while warm anomalies over mid-latitude North Pacific are clearly

378 seen only in SEAS5.1-03 (Fig. 4h). The AMV exhibits strong fluctuations in both the sign and values of the 11-year moving

379 window trend, which are well represented by the bootstrapped SEAS5.1-03 ensemble (Fig. 4l).

380 Note that both AMV and Snow-NAm SEAS5.1 indices are more tightly constrained than other indices. This because SST or

381 snow cover fields are characterized by larger inertia and have a slower variability than atmospheric fields, such as T2m or

382 Z500. The next will assess the relationships among these indices and GBI.

| Deleted: is due to the fact that |

384
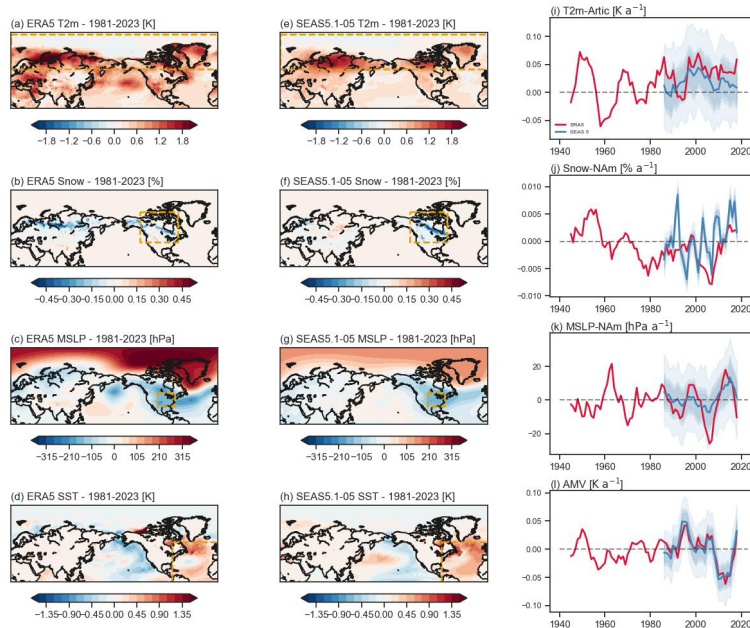
Figure 4. Composites and 11-year moving window trend of monthly indices. Panel (a) shows the composites of JJA T2m fields for months with T2m-Arctic > 1 s.d. for ERA5-81. Panel (b) same as for Panel (a) but for snow coverage in May during months with Snow-NAm < 1 s.d.. Panel (c) as for Panel (a) but for MSLP fields during months with MSLP-NAm < 1 s.d.. Panel (d) as for Panel (a) but for SST fields during months with AMV > 1 s.d.. Panels (e)-(h) same as for panels (a)-(d) but for SEAS5.1-05. For each panel, the yellow dashed box in (a-h) indicates the area from which the monthly indices (T2m-Arctic, Snow-NAm, MSLP-NAm, AMV) were derived. Panels (i) illustrates the 11-year moving window trend of T2m-Arctic for ERA5 (red) and the SEAS5.1-05 distribution of 10⁴ timeseries in blue shades. Panels (j)-(l) same as for panel (i) but for Snow-NAm, MSLP-NAm, and AMV. The thick blue line indicates the median value of the total distribution. The grey dashed line indicates the moving window trend of ~0.

393

3.3 Relationship among climate drivers and blocking indices

Following the characterization of the potential GBI drivers from Section 3.2, we would like to assess their actual relationship with Greenland Blocking in both ERA5 and SEAS5.1. Indeed, one of the goals of this study is to test the Preece et al. (2023) hypothesis, hereafter referred to as "Preece23", which suggests that Arctic warming may induce early snow cover depletion in May over North America, generating a low-pressure anomaly, which in turn could act as a waveguide, leading to blocking over Greenland. Additionally, we aim to assess whether summer Greenland blocking is influenced by the AMV and evaluate SEAS5.1's ability to replicate the observed correlations. To investigate the relationship between various blocking indices (GBI, GGI, GHGS, GHGN) and key climate drivers (AMV, T2M-Arctic, Snow-NAm, MSLP-NAm, whose properties have been assessed in the previous section), we calculate a correlation heatmap using detrended variables from ERA5-40, ERA5-81, and SEAS5.1-03 (Fig. 5). All the time series are linearly detrended, except for ERA5-40 T2M-Arctic, which is detrended using a polynomial function due to its non-linear trend.

We first focus on the GBI index in relation to Preece23's hypothesis. In ERA5-81, positive (lag 0) correlations are found between both T2M-Arctic, MSLP-NAm and GBI ($r \sim 0.3$), while Snow-NAm (taken in May) shows a negative correlation with GBI ($r \sim -0.2$). Conversely, the correlation between AMV and GBI is $r \sim 0$. However, only the correlation between T2M-Arctic and GBI is statistically significant ($p < 0.05$), supporting only the first part of the hypothesis linking Arctic warming to enhanced GBI (Fig. 5b).

When comparing the original blocking index (GBI) to the derived GGI, the correlation values are qualitatively similar with some differences: the correlation between MSLP-NAm, T2m-Arctic and GGI decrease and are not significant for ERA5-81, while the correlation with Snow-NAm increases to a significant $r \sim 0.35$ (Fig. 5b). The correlation between GHGS and the precursors indices is qualitatively similar to that of GGI, with the difference that GHGS also shows a negative ($r \sim -0.3$) and significant correlation with MSLP-NAm. Interestingly, GHGS>0 is a requirement to have blocking over Greenland: however, the fact that this negative correlation does not show up for GBI and GGI may be because the correlation between GHGN and MSLP-NAm is also negative ($r \sim -0.5$), weakening the possible connection with blocking.

Indeed, GBI requires both GHGS and GHGN conditions to be met simultaneously, while GGI is a linear combination of the two. Thus, negative MSLP anomalies can lead to positive pressure anomalies over Greenland, which promote blocking (GHGS>0), but also negative pressure anomalies over eastern Greenland (GHGN>0), reducing the likelihood of blocking. As a result, the effects cancel out in GGI, leading to near-zero correlations with MSLP-NAm. Thus, disentangling the blocking indices into GHGS and GHGN reveals more details of the complex relationship between MSLP-NAm and Greenland blocking.

Extending the analysis to ERA5-40 generally results in weaker and less significant correlations, although qualitatively the sign of the correlation is consistent (Fig. 5a). Notably, the correlation between Snow-NAm, MSLP-NAm and GHGS and between Snow-NAm and GHGN are significant ($r \sim -0.2/0.3$, Fig. 5a). This suggests that the proposed Preece23 mechanism may not hold consistently over the complete available historical period. Two interpretations are possible: (i) Arctic warming may have

429 become more dominant only in recent decades and (ii) the stronger signal observed in ERA5-81 may result from sampling of
430 internal variability.

431 When the correlation between the potential drivers among each other is considered, both ERA-40 and ERA-81 generally show
432 consistent qualitative results (Figs. 5a and 5b respectively). Both AMV and T2m-Arctic exhibit negative correlations with
433 MSLP-NAm and Snow-NAm ($r \sim$ -0.1-0.4), while T2m-Arctic and AMV are positively correlated ($r \sim 0.3$). Snow-NAm and
434 MSLP-NAm are also positively correlated ($r \sim$ 0.1-0.4). However, the strength of these correlations varies between the periods,
435 with stronger correlations found in ERA5-81 (Fig. 5b). In general, no direct correlation is found between AMV and the
436 blocking indices, indicating that AMV's influence on blocking may be indirect, primarily acting through MSLP-NAm.

438 Finally, we assess whether SEAS5.1-03 can replicate the observed correlations (Fig. 5c). SEAS5.1-03 generally weaker
439 correlations, which are somehow expected given the usual small signal-to-noise ratio of prediction systems typical over the
440 North Atlantic sector (Scaife and Smith, 2018). The correlation values in Fig. 5c represents the median of the distribution for
441 each pair of time series, with standard deviations shown in Fig. S12 in the Supplementary Material. Despite this difference,
442 SEAS5.1-03 replicates key patterns, especially the correlations among AMV, T2M-Arctic, and Snow-NAm. The positive
443 correlation between T2m-Arctic and the blocking indices is weaker ($r \sim$ 0.1-0.2) but consistent with what is shown in ERA5-
444 81. In contrast, SEAS5.1-03 struggles to capture correlations between Snow-NAm, MSLP-NAm, and the blocking indices,
445 except for a weak negative correlation between MSLP-NAm and GHGS ($r \sim$ -0.2). As snow cover in SEAS5.1-03 is derived
446 from climate model variables rather than observational data, we test whether a later initialization in SEAS5.1 (closer to
447 observed snow cover) could improve these correlations (see Fig. S12 in the Supplementary Material). We examine SEAS5.1-
448 05, which uses ERA5.1 snow cover initialized on May 1, and SEAS5.1-06, which allows for snow cover over the entire month
449 of May as calculated in ERA5-81. While this later initialization strengthens correlations among the climate drivers,
450 unfortunately it does not improve their relationship with the blocking indices.

451 Thus, in ERA5 our findings generally support the first part of Preece23's hypothesis, showing that T2M-Arctic and May snow
452 cover may influence MSLP over North America, which in turn favours pressure highs over Greenland (GHGS>0). However,
453 this does not consistently lead to blocking, as MSLP also contributes to GHGN>0, reducing the likelihood of blocking. The
454 AMV appears to have a moderate influence on MSLP and Arctic temperature, potentially affecting blocking indirectly. While
455 SEAS5.1-03 to SEAS5.1-06 captures relationships among climate drivers similar to those seen in observational data, they fail
456 to replicate the full extent of snow cover's role in blocking indices, particularly in relation to MSLP. This suggests a potential
457 misrepresentation of the driver-blocking interactions in the model, or missing elements in snow field initialization. Using the
458 HA16 index leads to qualitatively similar results for both ERA5 and SEAS5.1 (see Fig. S13 in the Supplementary Material),
459 even though, as expected, some stronger relationship emerges for ERA5. Further analysis in the next Section will explore
460 causal relationships between these drivers and blocking indices.

461

462
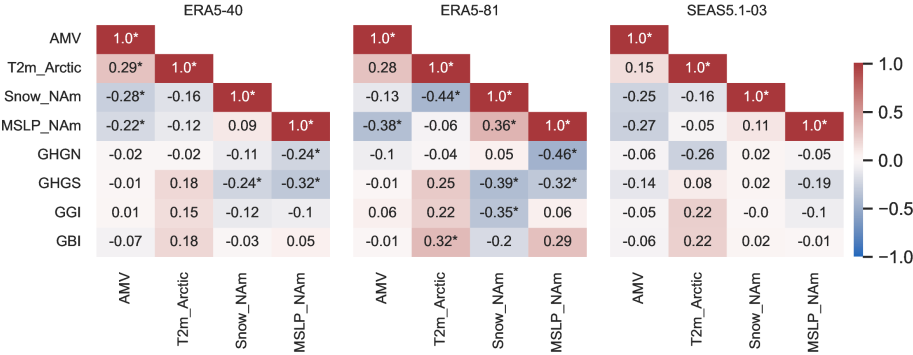
Figure 5. Summer correlation heat maps. Panel (a) shows the correlation of the different blocking indices (GBI, GGI, GHGS, GHGN) and the four identified potential monthly drivers (AMV, T2M-Arctic, Snow-NAm, MSLP-NAm) in ERA5-40 for the summer season. Panel (b) same as for panel (a) but for ERA5-81. Panel (c) same for panel (b) but for SEAS5.1-03. All data were linearly detrended except for T2M-Arctic in ERA5-40 which was detrended using a polynomial fit. Statistically significant values at p < 0.05 are marked with an asterisk. The SEAS5.1-03 correlation values represent the median correlations from the 10^4 bootstrapped samples. The correlations were analysed for summer (JJA averaged) for all variables, while snow cover data were taken from the monthly mean in May.

469

3.4 Causal relationship in ERA5 and SEAS5.1

To disentangle spurious correlations from causal relationships, we now apply PCMCI to detect the causal links between GGI and its potential drivers. First, we apply PCMCI to build a causal effect network (CEN) for monthly GGI, Snow-NAm, T2m-Arctic, MSLP-NAm and AMV. We use lag_{max} = -2 for ERA5-81 and lag_{max} = -1 for SEAS5.1-03 (this is necessary not to violate PCMCI requirements, see Methods Section 2.3), while lag_{min} is set to 0 for both ERA5-81 and SEAS5.1-03. Note that, given the shortness of the time series, we do not apply the FDR correction to ERA5-81, which would result in too few significant causal links. Thus, we use the obtained CENs not to make final statements about causal relationships, but rather to get a first reasonable estimate of the potential causal links and to provide a first comparison between ERA5-81 and SEAS5.1-03. The ERA5-81 CEN (Fig. 6a) shows two incoming causal links towards GGI at lag –2, one negative (β = -0.15) from Snow-NAm and one positive (β = 0.15) from T2m-Arctic. A negative undirected link (lag 0) between AMV and GGI is also present (β = -0.15). These links mean that lower than average Snow over North America during April-May-June (AMJ) is followed by higher than average GGI values in JJA. Similarly, though with opposite signs, higher than average T2m over the Arctic circle in AMJ are followed by higher than average GGI values in JJA. Thus, these links would support Preece23's hypothesis

483   that early snow cover depletion over North America can lead to more blocking. Similarly, the link from T2m-Arctic hints to

484   the potential relevance of Arctic warming for blocking. The undirected link between AMV and GGI shows that lower than

485   average AMV values in JJA correspond to higher than average GGI values in the same months. MSLP-NAm shows only one

486   incoming positive ($\beta = 0.15$) link from Snow-NAm at lag –2, meaning that higher than average Snow-NAm values in AMJ are

487   followed by higher MSLP anomalies over eastern North America, also in keeping with Preece23. Snow-NAm shows three

488   incoming links: one positive link from MSLP-NAm at lag –1 ($\beta = 0.15$), and two negative links, one from T2m-Arctic at lag

489   –1 ($\beta = -0.3$) and one from AMV at lag –2 from AMV ($\beta = -0.15$). Thus, higher than average Arctic temperatures and SST

490   over the North Atlantic are both followed by lower than average Snow anomalies in the following months, while higher than

491   average MSLP-NAm anomalies lead to higher Snow anomalies. Thus, Arctic warming has the potential to contribute to snow

492   depletion and in turn to increased blocking. T2m-Arctic shows only one incoming negative link at lag –2 ($\beta = 0.15$) from

493   Snow-NAm. Finally, AMV also shows only one positive incoming link at lag –1 from T2m-Arctic ($\beta = 0.15$).

494   The same CEN but for SEAS5.1-03 is shown in Fig. 6b. In general, a similar network structure is shown, with the following

495   differences: the GGI is connected to T2m-Arctic via a positive undirected link (lag 0, $\beta = 0.25$), to MSLP-NAm via a negative

496   undirected link (lag 0, $\beta = -0.15$) and to AMV by a negative undirected link (lag 0, $\beta = -0.1$). A direct link from Snow-NAm

497   is not present in SEAS5.1-03. The AMV shows one additional undirected link with MSLP-NAm (lag 0, $\beta = -0.1$) and two

498   negative incoming links at lag –1 from MSLP-NAm ($\beta = -0.1$) and GGI ($\beta = -0.1$). Two undirected links are also shown

499   between MSLP-NAm and Snow (lag 0, $\beta = 0.1$) and between the latter and T2m-Arctic (lag 0, $\beta = -0.1$). These results show

500   that ERA5-81 and SEAS5.1-03 generally agree on the causal links found among MSLP-NAm, Snow-NAm and T2m-Arctic.

501   However, the direct causal link from Snow-NAm towards GGI is missing, while the undirected link from MSLP-NAm appears.

502   Note that ERA5-81 and SEAS5.1-03 CEN are not one-to-one comparable, because (i) the maximum lag used is different, (ii)

503   the length of the two time series is different and (iii) a different set of causal precursors will by construction lead to different

504   β-values.

505   In general, similar causal links are also detected when GHGS, GHGN and the HA16 index are analysed (Figs. S14-15 in

506   Supplementary Material). For ERA5-81, most links are consistent with what shown in Fig. 6a, with the following differences:

507   (i) AMV and Snow-NAm are linked by a two-way negative causal link (Figs. S14a,b), (ii) the link from T2m-Arctic towards

508   GHGS is missing (Fig. S14a) and (iii) MSLP-NAm shows a direct link towards both GHGS and GHGN (Figs. S14a,b). For

509   SEAS5.1-03, again most links are consistent with what shown in Fig. 6b, with the following differences: (i) no direct link is

510   found between MSLP-NAm and GHGN (Fig. S14d) and (ii) GHGS shows two additionally outgoing links towards T2m-

511   Arctic and AMV (Fig. S14c). Note that GHGN links should have an opposite sign with respect to those shown for GHGS in

512   order to have the same effect on GGI. E.g. a positive (negative) influence of T2m-Arctic on GHGS (GHGN) has a joint positive

513   effect on GGI. In contrast, the negative effect of MSLP-NAm on both GHGS and GHGN (Figs. S14a-b) cancels out when

514   GGI is considered (Fig. 6a) meaning we do not find the proposed connection between the wave source (MLSP-NAm) and the

515   blocking (GGI, Fig. 6a) suggested by Preece23. However, given the direct link from snow cover to GHGS, but not to GHGN,

516   this relationship extends to GGI, supporting the hypothesis that early snow cover depletion in May might influence blocking

518 patterns. Although the direct association between the AMV and the blocking gradients is not observed, an indirect influence
519 is suggested through a connection with MSLP-NAm, indicating at least some level of natural variability affecting the blocking
520 indices GHGS and GHGN.

521 Thus, in general, the proposed chain of causality supports the idea that all four potential drivers influence, directly or indirectly,
522 blocking over Greenland. In keeping with Preece23, higher Arctic temperatures are linked to snow cover depletion, which is
523 in turn linked to negative MSLP anomalies over North America. While it is unclear whether these negative anomalies can lead
524 to blocking, their influence on the meridional gradients is apparent. A direct link from snow cover towards GGI is only found
525 in ERA5-81, while both model and reanalysis show a link to Arctic temperatures. The Atlantic multidecadal sea surface
526 temperature variability is also negatively affecting blocking over Greenland and indirectly GHGS and GHGN, supporting the
527 hypothesis that natural variability also plays a role.

528
529
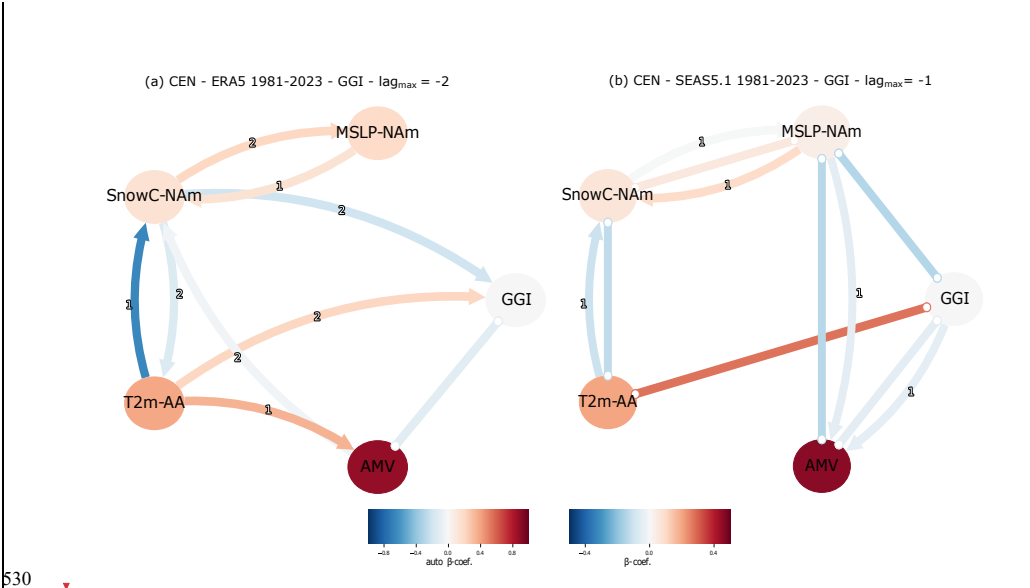
Figure 6. Causal effect networks for ERA5 and SEAS5.1-03. Panel (a): CEN with MSLP-NAm, Snow-NAm, T2m-Arctic, AMV and GGI for ERA5-81 and $\alpha = 0.05$ (no FDR applied, see Methods Section 2.3). Panel (b): same as for Panel (a) but for SEAS5.1-03 and with FDR correction applied. In each CEN, actors are represented by a node in the network, while lagged causal relationships are represented by directed arrows, showing the direction of causality. Lag 0 links are shown as straight arrows without an edge. The colour of the arrows

536 (nodes) shows the strength of the causal effect, the β value (auto β value), while the numbers on the arrows show the lag at which the causal
537 link is detected.
538

539 To provide a fair comparison between ERA5-81 and SEAS5.1-03, we adopt the concept of causal inference (see Methods
540 Section 2.3). Based on the results shown in Fig. 6, we now assume that the selection of causal links shown in Fig. 7a is found
541 in both ERA5-81 and SEAS5.1-03, and also for GHGS and GHGN indices. Here, we construct the CEN network by imposing
542 a sub-selection of all the links that PCMCI detects in Fig. 6a and 6b. Links are sub-selected to best represent the Preece23
543 hypothesis and to balance between links found in ERA5 and those found in SEAS5.1. Note that in Fig. 7a the maximum lag
544 used is -1. Moreover, while in Fig. 6b the sign of the SEAS5.1 MSLP-NAm → GGI link (lag 0) is negative, in ERA5 this link
545 shows a positive sign (Fig. 7a). Figures 7b-e show the β values calculated for ERA5-81 and ERA5-40, together with the β
546 value distributions obtained by bootstrapping 1000 times SEAS5.1-03 and SEAS.1-05. For links that do not include GGI (Fig.
547 7b), in general ERA5-81 and ERA5-40 β values fall inside the SEAS5.1-03 and SEAS.1-05 β value distributions. The AMV
548 → MSLP-NAm link (lag 0) show negative $\beta \sim$ -0.1-0.2, with SEAS5.1 showing somewhat higher absolute values up to $\beta \sim$ -
549 0.2 (Fig. 7b). The T2m-Arctic → Snow-NAm link (lag -1) shows the strongest causal effect with a $\beta \sim$ -0.3-0.5, however, both
550 ERA5 values are outside or at the far end of the two SEAS5.1 distributions, which are cantered around $\beta \sim$ -0.1-0.2. This hints
551 to a potential underestimation of the effect of MJJ Snow on JJA MSLP over North America in SEAS5.1. In contrast, the Snow-
552 NAm → T2m-Arctic link (lag -1) is cantered around $\beta \sim 0$ in both ERA5 and SEAS5.1, showing a negligible effect of North
553 American snow cover on Arctic surface temperatures. Both the Snow-NAm → MSLP-NAm link (lag -1) and the MSLP-NAm
554 → Snow-NAm link (lag -1) show a weak positive $\beta \sim$ 0.1-0.2 on each other, with the latter being somewhat stronger in
555 SEAS5.1.

556 Figures 7c, 7d and 7e show the causal links directed towards GGI, GHGS and GHGN respectively. For GGI, three links show
557 good agreement between ERA5 and SEAS5.1, i.e. AMV → GGI (lag 0, $\beta \sim$ -0.1), T2m-Arctic → GGI (lag 0, $\beta \sim$ 0.2-0.4) and
558 GGI → GGI itself (lag –1, $\beta \sim$ 0.1-0.2). For these links, ERA5 β values fall inside the distribution of SEAS5.1 β values. This
559 is not the case for links T2m-Arctic → GGI (lag -1, ERA5 $\beta \sim$ 0.3, SEAS5.1 $\beta \sim$ 0.1), Snow-NAm → GGI (lag -1, ERA5 $\beta \sim$
560 -0.2, SEAS5.1 $\beta \sim$ 0) and MSLP-NAm → GGI (lag 0, ERA5 $\beta \sim$ 0.1, SEAS5.1 $\beta \sim$ -0.2). For the latter, the (absolute) β values
561 are higher in SEAS5.1 than in ERA5, while SEAS5.1 struggles to reproduce the strength of the causal effect of Snow-NAm
562 and Arctic-T2m on GGI (Fig. 7c). GHGS (Fig. 7d) and GHGN (Fig. 7e) show similar results. However, when the two
563 components that make GGI are analysed separately, it is possible to distinguish whether the underestimation effect in SEAS5.1
564 comes from the southern or norther components of the blocking gradients. E.g., the underestimation of the GGI → Snow (lag
565 –1) link comes from an underestimation of the GHGS → Snow causal link (Fig. 7d), while the underestimation of the GGI →
566 T2m-Arctic (lag –1) link comes from an underestimation of the GHGN → T2m-Arctic link (Fig. 7e).
567 In general, for 7 out of the 11 causal links analyses there is a good match between ERA5 and SEAS5.1. However, SEAS5.1
568 seems to underestimate the links between both Arctic surface temperatures and snow cover over North America and blocking
569 indices (Fig. 7c-e). Moreover, the influence of snow cover on MSLP over North America is also underestimated (Fig. 7b).

570 Thus, the causal analysis supports the hypothesis that the forecast model does not correctly represent the physical effects of

571 depleted snow cover on increased blocking over Greenland. Using the HA16 index leads to qualitatively similar results (see

572 Fig. S16 in the Supplementary Material).
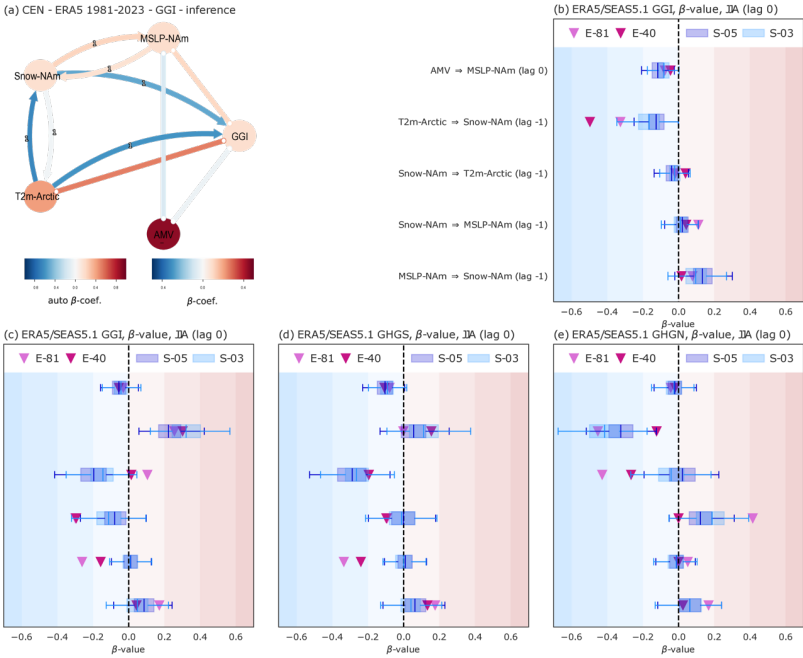
574 **Figure 7. Causal inference for monthly potential precursors.** Panel (a): inferred CEN with ERA5 MSLP-NAm, Snow-NAm, T2m-Arctic,
575 AMV and GGI for the 1981-2023 period for both SEAS5.1-03, SEAS5.1-05, ERA5-40 and ERA5-81. Panel (b): β values for links shown
576 in Panel (a) that do not include GGI. Panel (c): same as for Panel (b) but for links that are directed towards GGI. Panel (e) and (f): same as
577 for Panel (c) but for GHGS and GHGN indices. The boxplots show β values calculated a 1000 time in SEAS5.1-03 and SEAS5.1-05
578 (whiskers show the 95% confidence interval).

579 **4 Discussions and Conclusions**

580 In this study, we investigate whether the observed trend in summer Greenland blocking can be attributed to natural variability,

581 looking at features as the Atlantic multidecadal variability (AMV), or whether it is influenced by Arctic warming, following

582 the hypothesis proposed by Preece23. According to Preece23, Arctic warming may lead to early snow cover depletion in May,

583 which can generate a low-pressure anomaly over North America, which subsequently may act as a waveguide, resulting in
584 increased blocking over Greenland.

585 On top of this, our study aims to address a critical gap in understanding the representation of Greenland blocking within
586 advanced seasonal forecasting systems by evaluating the ECMWF SEAS5.1. Following the definition of Davini et al. (2012)
587 for the Greenland blocking index (GBI), we derived a Greenland gradient index (GGI) from its southern and northern
588 meridional components, GHGS and GHGN, to ensure a continuous time series for statistical analysis where the use of the GBI
589 was not applicable. Both blocking indices (GBI, GGI) show a positive statistically significant trend from 1940 to 2023 but
590 reveal a negative trend in the last decade. The analysis focuses on how SEAS5.1 state-of-the-art, multi-member high-resolution
591 model captures the spatial patterns, trends, and natural variability associated with Greenland blocking.

592 Using various statistical methods (linear regression, correlation analysis, causal discovery, and causal inference), we find
593 multiple evidence that both Arctic warming and natural variability have influenced Greenland blocking at monthly time scales
594 during the observational period. Our correlation and causal analyses indicate a robust relationship in ERA5, where high Arctic
595 temperatures lead to early snow cover depletion in May, which can subsequently cause a low-pressure anomaly over North
596 America (MSLP-NAm), consistent with Preece23 (Figs. 5, 6 and 7). The identified relationships are stronger over the more
597 recent time window 1981-2023 rather than the full reanalysis period 1940-2023: this is consistent with the larger impact of
598 Arctic warming in the recent years, which could have weakened the background westerly flow, and this favoured stronger
599 stationary wave persistence (Hoskins and Woollings, 2015; Coomou et al, 2018).

600 While in ERA5 the direct effect of MSLP-Nam on GGI seems limited (Fig. 7c), its effect on the meridional gradient reversal
601 GHGS is consistent with Preece23: negative MSLP-NAm leads to positive GHGS anomalies (Fig. 7d). However, negative
602 MSLP-NAm also leads to positive GHGN anomalies (Fig. 7e), likely explaining the lack of signal on GGI. Snow cover
603 influences MSLP-NAm (Figs. 6a and 7b), and shows a direct effect on GGI and GHGS, but not on GHGN. Enhanced Arctic
604 temperatures also positively influence GGI and GHGS, while GHGN receives a consistent negative influence (Figs. 7c-e).

605 Overall, our analysis reveals that in ERA5, higher Arctic temperatures and reduced snow cover are associated with low-
606 pressure anomalies over North America but do not result in blocking, as defined by the index used in our study. However, we
607 observe a connection with elevated pressure highs over Greenland (GHGS > 0). This finding aligns with Preece et al. (2023),
608 where the authors apply the HA16 blocking index proposed by Hanna et al., which defines blocking as a large geopotential
609 height value over Greenland (Hanna et al., 2013). Notably, the HA16 index lacks some characteristics typically associated
610 with blocking, being mostly the presence of a westerly flow poleward of the block. The degree of similarity between this index
611 and GHGS > 0, as well as whether it sufficiently captures Greenland blocking, remains an open question. Addressing this gap
612 could provide valuable insights and warrants further investigation in future studies.

613

614 When focusing on SEAS5.1, it is possible to see that even with some difficulties the model can reproduce the observed blocking
615 trend (only ~10% of the sub-samples show a trend that is comparable with the ERA5 trend, Fig. 2). The forecast system shows
616 consistent causal links among high Arctic temperatures, low snow cover, and low-pressure over North America (Figs. 6b and

620   7b), which agree both with ERA5 and with the Preece23 hypothesis, although the strength of these connections is generally

621   underestimated in the model, suggesting a low signal-to-noise ratio. However, the influence of snow cover on the blocking

622   indices is the most misrepresented causal link (Figs. 7c-e). Thus, this suboptimal mechanism may explain the difficulties of

623   SEAS5.1 to replicate the historical trends in ERA5.

624   The culprit might be the misrepresentation of snow cover in SEAS5.1: May snow cover climatology in SEAS5.1 shows an

625   overestimation over western North America both in SEAS5.1-03 and SEAS.1-05 (see Supplementary Material Figs. S10o and

626   S11o respectively). This hypothesis is also supported by the strong differences in the 11-year running mean between ERA5

627   and SEAS5.1 (Fig. 4j). While SEAS5.1 data initialized in March and May shows very similar causal results (Fig. 7), using

628   SEAS5.1 initialised in June, improves at least partially the correlations among Arctic temperatures, snow cover, and low-

629   pressure over North America (Fig. S8). However, it does not improve the correlations with the blocking indices, suggesting

630   that even using snow cover values closer to the observations does not improve the representation of the snow – blocking link

631   in SEAS5.1.

632   While blocking shows multidecadal variability in its observed blocking trends, the influence of the Atlantic multidecadal

633   variability (AMV) on blocking variability is only weakly detected. The 11-year moving window trends in the blocking indices

634   (Fig. 2) and their potential drivers (Fig. 4) indicate strong variability over the observational period. The AMV shows a

635   negligible causal influence on blocking indices (Fig. 7c-e). Nevertheless, AMV has at least some influence on the pressure-

636   low and snow cover over North America (though the latter is found only on ERA5, Fig. 6), and thus has an indirect, though

637   weak, influence over blocking. The AMV shifted to a positive trend in 1981, likely enhancing the negative trend of MSLP

638   and, in turn, blocking trends. Thus, our analysis shows that the combination of high Arctic warming and a positive AMV phase

639   likely favour enhanced blocking over Greenland. However, in the past six years, we observed a weakening in the blocking

640   trend (Fig. 2), despite a steady increase in Arctic temperature and decrease in low-pressure over North America (Figs. 4j and

641   4k respectively), indicating that internal variability might be overshadowing the Arctic warming signal. In fact, in that same

642   period a small positive trend in the Snow cover of North America was observed, which could explain the dampening of the

643   blocking. If this mechanism holds, we could further speculate in the short-term that the positive phases of the AMV will

644   enhance the probability of low pressure over North America, thereby increasing both GHGS and GHGN. However, if snow

645   cover will continue to decrease, positive values of GHGS may prevail, favouring larger blocking frequencies.

646

647   Blocking is important for Greenland surface temperatures and Greenland melting events (Hanna et al., 2018; McLeod and

648   Mote, 2016; Sasgen et al., 2020). Thus, the uncertainty in how climate models can reproduce blocking variability and trends

649   (Delhasse et al., 2020; Maddison et al., 2024) represents a challenge to correctly estimate the future changes that will affect

650   the Greenland ice sheet. Our analysis builds confidence that the ECMWF seasonal forecasting system can reproduce, though

651   rarely, the observed trend, highlighting the limitation of CMIP6 where none of the models is able to replicate the trend.

652   Moreover, the seasonal forecast model can represent most of the Arctic – blocking links, apart from the direct link of snow

653   cover on blocking. Thus, while blocking over Greenland does not show increasing trends in future projections (Davini and

656 D'Andrea, 2020), we show that there is a reasonable chance that the lack of this trend is explained by suboptimal representation
657 of the snow – blocking mechanisms in the model.

658 Future changes in the causal drivers of blocking can then provide us with an estimation of the potential effect that these changes
659 may have on blocking itself. Snow cover extent over North America will keep declining (O'Gorman, 2014; Quante et al.,
660 2021) while Arctic temperatures are projected to keep increasing under anthropogenic climate change (Cai et al., 2021; Hu et
661 al., 2021; Shu et al., 2022). This combined effect has the potential to contribute to increased blocking over Greenland and then
662 accelerate melting of its ice sheet. However, the amount of snowfall in winter is probably influenced by large-scale oceanic
663 and atmospheric patterns (Lundquist et al., 2023) meaning that climate variability will continue to influence blocking. Thus,
664 while blocking will still be modulated by the AMV or other sources of natural variability, in the long term, snow cover will
665 decline due to the dominant forces of climate change, potentially leading to increased blocking. Of course, changes in tropical
666 regions, or changes in these teleconnection pathways (Meehl et al., 2018a, Zhu et al., 2024) can potentially enhance the effect
667 of climate change in Arctic regions: however, it is worth mentioning that we explored the potential linkage between El Niño
668 Southern Oscillation (ENSO) making use of the PCMCI methodology and no evident linkage emerges between the NINO3.4
669 index and any of the Greenland blocking used.

670

671 To summarize, we investigated the role of snow cover over North America, Arctic amplification and Atlantic multidecadal
672 variability in influencing Greenland blocking trends. Our findings suggest that higher Arctic temperatures lead to early snow
673 cover depletion, causing low-pressure anomalies over North America, which may increase blocking over Greenland, in
674 alignment with the theory proposed by Preece et al (2023).

675 On top of this, this work looks at different components of Greenland blocking, thus identifying the specific effect of each
676 causal driver on both its southern and northern meridional components. The ECMWF SEAS5.1 model struggles to accurately
677 represent the causal links between Arctic temperatures, snow cover, and surface pressure patterns, potentially limiting its
678 ability to reproduce observed blocking trends. Indeed, SEAS5.1 can reproduce the Arctic temperature – snow cover – low
679 pressure links while struggling in reproducing the direct causal link between snow cover and Greenland blocking, hinting at a
680 potential missing physical mechanism that may explain the discrepancy between observed and modelled trends.

681 However, a negative blocking trend in the last decade challenges the idea that Arctic warming is the main driver of changes in
682 atmospheric blocking over Greenland. Thus, the recent decline in the observed blocking trend, despite stable Arctic
683 temperature increases, indicates that other factors may be at play. Despite the above-mentioned limitations, SEAS5.1 can
684 reproduce the observed Greenland blocking trend in only 10% of its samples but does not rule entirely the possibility that
685 natural variability is playing a considerable role in the current observed trend of summer Greenland blocking. This of course
686 opens the question to what extent such linkage might be affecting other regions in the high latitudes and offsetting other long-
687 term predictions in global climate models. Future work is needed to further assess the capability of historical and future
688 projections provided by CMIP6 models in representing this snow – blocking mechanisms, to evaluate the reliability of future
689 trends in blocking over Greenland.

Data availability. The data used in this article can be accessed by contacting the corresponding author. ERA5 (https://doi.org/10.24381/cds.50ed0a73, Copernicus Climate Change Service, Climate Data Store, 2018) and SEAS5.1 (https://doi.org/10.24381/cds.adbb2d47, Hersbach et al., 2023) datasets are publicly available on the Copernicus website.

Supplement. The supplement related to this article is available.

Author contributions. J.B., G.D.C. and P.D. equally contributed to the design of the analysis. J.B. and G.D.C. performed the analysis and wrote the first draft of the paper. J.B., G.D.C. and P.D. contributed to the interpretation of the results and to the writing of the paper.

Competing interests. The contact author has declared that none of the authors has any competing interests.

Acknowledgements. We thank Efi Rousi and Fabio D'Andrea for the valuable discussions at the onset of this research project.

Financial support. This research has been supported by the German Federal Ministry for Education and Research (BMBF) via the JPI Climate/JPI Oceans project ROADMAP (grant no. 01LP2002B) (G.D.C.) and via the ClimXtreme project (subproject PERSEVERE, phase 2nd, grant no. 01LP2322D) (G.D.C.). J.B. was further supported by the Australian Research Council Special Research Initiative Securing Antarctica's Environmental Future (SR200100005).

References

Baxter, I., Ding, Q., Schweiger, A., L'Heureux, M., Baxter, S., Wang, T., Zhang, Q., Harnos, K., Markle, B., Topal, D., and Lu, J.: How Tropical Pacific Surface Cooling Contributed to Accelerated Sea Ice Melt from 2007 to 2012 as Ice Is Thinned by Anthropogenic Forcing, Journal of Climate, 32, 8583–8602, https://doi.org/10.1175/JCLI-D-18-0783.1, 2019.

Beckmann, J. and Winkelmann, R.: Effects of extreme melt events on ice flow and sea level rise of the Greenland Ice Sheet, The Cryosphere, 17, 3083–3099, https://doi.org/10.5194/tc-17-3083-2023, 2023.

Benjamini, Y. and Hochberg, Y.: Controlling the False Discovery Rate: A Practical and Powerful Approach to Multiple Testing, Journal of the Royal Statistical Society. Series B (Methodological), 57, 289–300, https://doi.org/10.2307/2346101, 1995.

Blackport, R. and Screen, J. A.: Insignificant effect of Arctic amplification on the amplitude of midlatitude atmospheric waves, Sci. Adv., 6, eaay2880, https://doi.org/10.1126/sciadv.aay2880, 2020.

Blau, M. T., Ha, K.-J., and Chung, E.-S.: Extreme summer temperature anomalies over Greenland largely result from clear-sky radiation and circulation anomalies, Commun Earth Environ, 5, 405, https://doi.org/10.1038/s43247-024-01549-7, 2024.

Bracegirdle, T. J.: Early-to-Late Winter 20th Century North Atlantic Multidecadal Atmospheric Variability in Observations, CMIP5 and CMIP6, Geophysical Research Letters, 49, e2022GL098212, https://doi.org/10.1029/2022GL098212, 2022.

Cai, W., Santoso, A., Wang, G., Yeh, S.-W., An, S.-I., Cobb, K. M., Collins, M., Guilyardi, E., Jin, F.-F., Kug, J.-S., Lengaigne, M., McPhaden, M. J., Takahashi, K., Timmermann, A., Vecchi, G., Watanabe, M., and Wu, L.: ENSO and greenhouse warming, Nature Clim Change, 5, 849–859, https://doi.org/10.1038/nclimate2743, 2015.

Cai, Z., You, Q., Wu, F., Chen, H. W., Chen, D., and Cohen, J.: Arctic Warming Revealed by Multiple CMIP6 Models: Evaluation of Historical Simulations and Quantification of Future Projection Uncertainties, Journal of Climate, 34, 4871–4892, https://doi.org/10.1175/JCLI-D-20-0791.1, 2021.

Di Capua, G., Sparrow, S., Kornhuber, K., Rousi, E., Osprey, S., Wallom, D., van den Hurk, B., and Coumou, D.: Drivers behind the summer 2010 wave train leading to Russian heatwave and Pakistan flooding, npj Climate and Atmospheric Science, 4, https://doi.org/10.1038/s41612-021-00211-9, 2021.

Cellitti, M. P., Walsh, J. E., Rauber, R. M., and Portis, D. H.: Extreme cold air outbreaks over the United States, the polar vortex, and the large-scale circulation, J. Geophys. Res., 111, 2005JD006273, https://doi.org/10.1029/2005JD006273, 2006.

Chen, L., Li, T., Yu, Y., and Behera, S. K.: A possible explanation for the divergent projection of ENSO amplitude change under global warming, Clim Dyn, 49, 3799–3811, https://doi.org/10.1007/s00382-017-3544-x, 2017.

Cohen, J., Screen, J. A., Furtado, J. C., Barlow, M., Whittleston, D., Coumou, D., Francis, J., Dethloff, K., Entekhabi, D., Overland, J., and Jones, J.: Recent Arctic amplification and extreme mid-latitude weather, Nature Geosci, 7, 627–637, https://doi.org/10.1038/ngeo2234, 2014.

Cohen, J., Zhang, X., Francis, J., Jung, T., Kwok, R., Overland, J., Ballinger, T. J., Bhatt, U. S., Chen, H. W., Coumou, D., Feldstein, S., Gu, H., Handorf, D., Henderson, G., Ionita, M., Kretschmer, M., Laliberte, F., Lee, S., Linderholm, H. W., Maslowski, W., Peings, Y., Pfeiffer, K., Rigor, I., Semmler, T., Stroeve, J., Taylor, P. C., Vavrus, S., Vihma, T., Wang, S., Wendisch, M., Wu, Y., and Yoon, J.: Divergent consensuses on Arctic amplification influence on midlatitude severe winter weather, Nat. Clim. Chang., 10, 20–29, https://doi.org/10.1038/s41558-019-0662-y, 2020.

Collins, M., Beverley, J. D., Bracegirdle, T. J., Catto, J., McCrystall, M., Dittus, A., Freychet, N., Grist, J., Hegerl, G. C., Holland, P. R., Holmes, C., Josey, S. A., Joshi, M., Hawkins, E., Lo, E., Lord, N., Mitchell, D., Monerie, P.-A., Priestley, M. D. K., Scaife, A., Screen, J., Senior, N., Sexton, D., Shuckburgh, E., Siegert, S., Simpson, C., Stephenson, D. B., Sutton, R., Thompson, V., Wilcox, L. J., and Woollings, T.: Emerging signals of climate change from the equator to the poles: new insights into a warming world, Front. Sci., 2, 1340323, https://doi.org/10.3389/fsci.2024.1340323, 2024.

Coumou, D., Di Capua, G., Vavrus, S., Wang, L., and Wang, S.: The influence of Arctic amplification on mid-latitude summer circulation, Nat Commun, 9, 2959, https://doi.org/10.1038/s41467-018-05256-8, 2018.

Davini, P. and D'Andrea, F.: Northern Hemisphere Atmospheric Blocking Representation in Global Climate Models: Twenty Years of Improvements?, Journal of Climate, 29, 8823–8840, https://doi.org/10.1175/JCLI-D-16-0242.1, 2016.

Davini, P. and D'Andrea, F.: From CMIP3 to CMIP6: Northern Hemisphere Atmospheric Blocking Simulation in Present and Future Climate, Journal of Climate, 33, 10021–10038, https://doi.org/10.1175/JCLI-D-19-0862.1, 2020.

Davini, P., Cagnazzo, C., Gualdi, S., and Navarra, A.: Bidimensional Diagnostics, Variability, and Trends of Northern Hemisphere Blocking, Journal of Climate, 25, 6496–6509, https://doi.org/10.1175/JCLI-D-12-00032.1, 2012.

Davini, P., Weisheimer, A., Balmaseda, M., Johnson, S. J., Molteni, F., Roberts, C. D., Senan, R., and Stockdale, T. N.: The representation of winter Northern Hemisphere atmospheric blocking in ECMWF seasonal prediction systems, Quart J Royal Meteoro Soc, 147, 1344–1363, https://doi.org/10.1002/qj.3974, 2021.

Davy, R., Chen, L., and Hanna, E.: Arctic amplification metrics, Intl Journal of Climatology, 38, 4384–4394, https://doi.org/10.1002/joc.5675, 2018.

Delhasse, A., Hanna, E., Kittel, C., and Fettweis, X.: Brief communication: CMIP6 does not suggest any circulation change over Greenland in summer by 2100, Ice sheets/Atmospheric Interactions, https://doi.org/10.5194/tc-2019-332, 2020.

Di Capua, G. and Coumou, D.: Changes in meandering of the Northern Hemisphere circulation, Environ. Res. Lett., 11, 094028, https://doi.org/10.1088/1748-9326/11/9/094028, 2016.

Di Capua, G., Kretschmer, M., Runge, J., Alessandri, A., Donner, R. V., Van Den Hurk, B., Vellore, R., Krishnan, R., and Coumou, D.: Long-Lead Statistical Forecasts of the Indian Summer Monsoon Rainfall Based on Causal Precursors, Weather and Forecasting, 34, 1377–1394, https://doi.org/10.1175/WAF-D-19-0002.1, 2019.

Di Capua, G., Runge, J., Donner, R. V., Van Den Hurk, B., Turner, A. G., Vellore, R., Krishnan, R., and Coumou, D.: Dominant patterns of interaction between the tropics and mid-latitudes in boreal summer: causal relationships and the role of timescales, Weather Clim. Dynam., 1, 519–539, https://doi.org/10.5194/wcd-1-519-2020, 2020a.

Di Capua, G., Kretschmer, M., Donner, R. V., Van Den Hurk, B., Vellore, R., Krishnan, R., and Coumou, D.: Tropical and mid-latitude teleconnections interacting with the Indian summer monsoon rainfall: a theory-guided causal effect network approach, Earth Syst. Dynam., 11, 17–34, https://doi.org/10.5194/esd-11-17-2020, 2020b.

Di Capua, G., Coumou, D., Van Den Hurk, B., Weisheimer, A., Turner, A. G., and Donner, R. V.: Validation of boreal summer tropical–extratropical causal links in seasonal forecasts, Weather Clim. Dynam., 4, 701–723, https://doi.org/10.5194/wcd-4-701-2023, 2023.

Di Capua, G., Tyrlis, E., Matei, D., and Donner, R. V.: Tropical and mid-latitude causal drivers of the eastern Mediterranean Etesians during boreal summer, Clim Dyn, 62, 9565–9585, https://doi.org/10.1007/s00382-024-07411-y, 2024.

Ding, Q., Wallace, J. M., Battisti, D. S., Steig, E. J., Gallant, A. J. E., Kim, H.-J., and Geng, L.: Tropical forcing of the recent rapid Arctic warming in northeastern Canada and Greenland, Nature, 509, 209–212, https://doi.org/10.1038/nature13260, 2014.

Diro, G. T. and Sushama, L.: Contribution of Snow Cover Decline to Projected Warming Over North America, Geophysical Research Letters, 47, e2019GL084414, https://doi.org/10.1029/2019GL084414, 2020.

Docquier, D., Di Capua, G., Donner, R. V., Pires, C. A. L., Simon, A., and Vannitsem, S.: A comparison of two causal methods in the context of climate analyses, Nonlin. Processes Geophys., 31, 115–136, https://doi.org/10.5194/npg-31-115-2024, 2024.

Feldstein, S. B.: The Timescale, Power Spectra, and Climate Noise Properties of Teleconnection Patterns, J. Climate, 13, 4430–4440, https://doi.org/10.1175/1520-0442(2000)013<4430:TTPSAC>2.0.CO;2, 2000.

Francis, J. and Skific, N.: Evidence linking rapid Arctic warming to mid-latitude weather patterns, Phil. Trans. R. Soc. A., 373, 20140170, https://doi.org/10.1098/rsta.2014.0170, 2015.

Francis, J. A. and Vavrus, S. J.: Evidence for a wavier jet stream in response to rapid Arctic warming, Environ. Res. Lett., 10, 014005, https://doi.org/10.1088/1748-9326/10/1/014005, 2015.

796 Gan, R., Huang, G., and Hu, K.: The Diverse Impacts of El Niño on Northeastern Canada and Greenland Surface Air
797 Temperatures, Journal of Climate, 37, 335–348, https://doi.org/10.1175/JCLI-D-22-0677.1, 2024.

798 Gollan, G., Greatbatch, R. J., and Jung, T.: Origin of variability in Northern Hemisphere winter blocking on interannual to
799 decadal timescales, Geophysical Research Letters, 42, https://doi.org/10.1002/2015GL066572, 2015.

800 Häkkinen, S., Rhines, P. B., and Worthen, D. L.: Atmospheric Blocking and Atlantic Multidecadal Ocean Variability, Science,
801 334, 655–659, https://doi.org/10.1126/science.1205683, 2011.

802 Hanna, E., Cropper, T.E., Hall, R.J. and Cappelen, J. (2016), Greenland Blocking Index 1851–2015: a regional climate change
803 signal. Int. J. Climatol., 36: 4847-4861. https://doi.org/10.1002/joc.4673

804 Hanna, E., Jones, J. M., Cappelen, J., Mernild, S. H., Wood, L., Steffen, K., and Huybrechts, P.: The influence of North Atlantic
805 atmospheric and oceanic forcing effects on 1900–2010 Greenland summer climate and ice melt/runoff, Intl Journal of
806 Climatology, 33, 862–880, https://doi.org/10.1002/joc.3475, 2013.

807 Hanna, E., Fettweis, X., Mernild, S. H., Cappelen, J., Ribergaard, M. H., Shuman, C. A., Steffen, K., Wood, L., and Mote, T.
808 L.: Atmospheric and oceanic climate forcing of the exceptional Greenland ice sheet surface melt in summer 2012, Intl Journal
809 of Climatology, 34, 1022–1037, https://doi.org/10.1002/joc.3743, 2014.

810 Hanna, E., Fettweis, X., and Hall, R. J.: Brief communication: Recent changes in summer Greenland blocking captured by
811 none of the CMIP5 models, The Cryosphere, 12, 3287–3292, https://doi.org/10.5194/tc-12-3287-2018, 2018.

812 Hauser, S., Teubler, F., Riemer, M., Knippertz, P., and Grams, C. M.: Life cycle dynamics of Greenland blocking from a
813 potential vorticity perspective, Weather Clim. Dynam., 5, 633–658, https://doi.org/10.5194/wcd-5-633-2024, 2024.

814 Hersbach, H., Bell, B., Berrisford, P., Hirahara, S., Horányi, A., Muñoz-Sabater, J., Nicolas, J., Peubey, C., Radu, R., Schepers,
815 D., Simmons, A., Soci, C., Abdalla, S., Abellan, X., Balsamo, G., Bechtold, P., Biavati, G., Bidlot, J., Bonavita, M., De Chiara,
816 G., Dahlgren, P., Dee, D., Diamantakis, M., Dragani, R., Flemming, J., Forbes, R., Fuentes, M., Geer, A., Haimberger, L.,
817 Healy, S., Hogan, R. J., Hólm, E., Janisková, M., Keeley, S., Laloyaux, P., Lopez, P., Lupu, C., Radnoti, G., De Rosnay, P.,
818 Rozum, I., Vamborg, F., Villaume, S., and Thépaut, J.: The ERA5 global reanalysis, Quart J Royal Meteoro Soc, 146, 1999–
819 2049, https://doi.org/10.1002/qj.3803, 2020.

820 Hoskins, B., & Woollings, T. (2015). Persistent Extratropical Regimes and Climate Extremes. Current Climate Change
821 Reports, 1(3), 115–124. https://doi.org/10.1007/s40641-015-0020-8

822 Hu, C., Yang, S., Wu, Q., Li, Z., Chen, J., Deng, K., Zhang, T., and Zhang, C.: Shifting El Niño inhibits summer Arctic
823 warming and Arctic sea-ice melting over the Canada Basin, Nat Commun, 7, 11721, https://doi.org/10.1038/ncomms11721,
824 2016.

825 Hu, X.-M., Ma, J.-R., Ying, J., Cai, M., and Kong, Y.-Q.: Inferring future warming in the Arctic from the observed global
826 warming trend and CMIP6 simulations, Advances in Climate Change Research, 12, 499–507,
827 https://doi.org/10.1016/j.accre.2021.04.002, 2021.

828 Johnson, S. J., Stockdale, T. N., Ferranti, L., Balmaseda, M. A., Molteni, F., Magnusson, L., Tietsche, S., Decremer, D.,
829 Weisheimer, A., Balsamo, G., Keeley, S. P. E., Mogensen, K., Zuo, H., and Monge-Sanz, B. M.: SEAS5: the new ECMWF
830 seasonal forecast system, Geosci. Model Dev., 12, 1087–1117, https://doi.org/10.5194/gmd-12-1087-2019, 2019.

831 Kohyama, T., Hartmann, D. L., and Battisti, D. S.: La Niña–like Mean-State Response to Global Warming and Potential
832 Oceanic Roles, Journal of Climate, 30, 4207–4225, https://doi.org/10.1175/JCLI-D-16-0441.1, 2017.

833 Kretschmer, M., Coumou, D., Donges, J. F., and Runge, J.: Using Causal Effect Networks to Analyze Different Arctic Drivers
834 of Midlatitude Winter Circulation, Journal of Climate, 29, 4069–4081, https://doi.org/10.1175/JCLI-D-15-0654.1, 2016.

835 Kretschmer, M., Coumou, D., Agel, L., Barlow, M., Tziperman, E., and Cohen, J.: More-Persistent Weak Stratospheric Polar
836 Vortex States Linked to Cold Extremes, Bulletin of the American Meteorological Society, 99, 49–60,
837 https://doi.org/10.1175/BAMS-D-16-0259.1, 2018a.

838 Kretschmer, M., Cohen, J., Matthias, V., Runge, J., and Coumou, D.: The different stratospheric influence on cold-extremes
839 in Eurasia and North America, npj Clim Atmos Sci, 1, 44, https://doi.org/10.1038/s41612-018-0054-4, 2018b.

840 Lehmann, J., Kretschmer, M., Schauberger, B., and Wechsung, F.: Potential for Early Forecast of Moroccan Wheat Yields
841 Based on Climatic Drivers, Geophysical Research Letters, 47, e2020GL087516, https://doi.org/10.1029/2020GL087516,
842 2020.

843 Liu, J., Chen, Z., Francis, J., Song, M., Mote, T., and Hu, Y.: Has Arctic Sea Ice Loss Contributed to Increased Surface Melting
844 of the Greenland Ice Sheet?, Journal of Climate, 29, 3373–3386, https://doi.org/10.1175/JCLI-D-15-0391.1, 2016.

845 Lundquist, J. D., Kim, R. S., Durand, M., and Prugh, L. R.: Seasonal Peak Snow Predictability Derived From Early-Season
846 Snow in North America, Geophysical Research Letters, 50, e2023GL103802, https://doi.org/10.1029/2023GL103802, 2023.

847 Luu, L. N., Hanna, E., De Alwis Pitts, D., Maddison, J., Screen, J. A., Catto, J. L., and Fettweis, X.: Greenland summer
848 blocking characteristics: an evaluation of a high-resolution multi-model ensemble, Clim Dyn, 62, 10503–10523,
849 https://doi.org/10.1007/s00382-024-07453-2, 2024.

850 Maddison, J. W., Catto, J. L., Hanna, E., Luu, L. N., and Screen, J. A.: Missing Increase in Summer Greenland Blocking in
851 Climate Models, Geophysical Research Letters, 51, e2024GL108505, https://doi.org/10.1029/2024GL108505, 2024.

852 Masato, G., Hoskins, B. J., and Woollings, T.: Winter and Summer Northern Hemisphere Blocking in CMIP5 Models, Journal
853 of Climate, 26, 7044–7059, https://doi.org/10.1175/JCLI-D-12-00466.1, 2013.

854 Matsumura, S. and Kosaka, Y.: Arctic–Eurasian climate linkage induced by tropical ocean variability, Nat Commun, 10, 3441,
855 https://doi.org/10.1038/s41467-019-11359-7, 2019.

856 Matsumura, S., Yamazaki, K., and Suzuki, K.: Slow-down in summer warming over Greenland in the past decade linked to
857 central Pacific El Niño, Commun Earth Environ, 2, 257, https://doi.org/10.1038/s43247-021-00329-x, 2021.

858 McCrystall, M. R., Stroeve, J., Serreze, M., Forbes, B. C., and Screen, J. A.: New climate models reveal faster and larger
859 increases in Arctic precipitation than previously projected, Nat Commun, 12, 6765, https://doi.org/10.1038/s41467-021-
860 27031-y, 2021.

861 McGraw, M. C. and Barnes, E. A.: New Insights on Subseasonal Arctic–Midlatitude Causal Connections from a Regularized
862 Regression Model, Journal of Climate, 33, 213–228, https://doi.org/10.1175/JCLI-D-19-0142.1, 2020.

863 McLeod, J. T. and Mote, T. L.: Linking interannual variability in extreme Greenland blocking episodes to the recent increase
864 in summer melting across the Greenland ice sheet: EXTREME GREENLAND BLOCKING AND SUMMER MELTING
865 ACROSS THE GREENLAND ICE SHEET, Int. J. Climatol., 36, 1484–1499, https://doi.org/10.1002/joc.4440, 2016.

866 Meehl, G. A., Chung, C. T. Y., Arblaster, J. M., Holland, M. M., and Bitz, C. M.: Tropical Decadal Variability and the Rate
867 of Arctic Sea Ice Decrease, Geophysical Research Letters, 45, https://doi.org/10.1029/2018GL079989, 2018.

Mudryk, L., Santolaria-Otín, M., Krinner, G., Ménégoz, M., Derksen, C., Brutel-Vuilmet, C., Brady, M., and Essery, R.: Historical Northern Hemisphere snow cover trends and projected changes in the CMIP6 multi-model ensemble, The Cryosphere, 14, 2495–2514, https://doi.org/10.5194/tc-14-2495-2020, 2020.

Nakamura, T., Yamazaki, K., Iwamoto, K., Honda, M., Miyoshi, Y., Ogawa, Y., Tomikawa, Y., and Ukita, J.: The stratospheric pathway for Arctic impacts on midlatitude climate, Geophysical Research Letters, 43, 3494–3501, https://doi.org/10.1002/2016GL068330, 2016.

Nghiem, S. V., Hall, D. K., Mote, T. L., Tedesco, M., Albert, M. R., Keegan, K., Shuman, C. A., DiGirolamo, N. E., and Neumann, G.: The extreme melt across the Greenland ice sheet in 2012, Geophys. Res. Lett., 39, 2012GL053611, https://doi.org/10.1029/2012GL053611, 2012.

Nowack, P., Runge, J., Eyring, V., and Haigh, J. D.: Causal networks for climate model evaluation and constrained projections, Nat Commun, 11, 1415, https://doi.org/10.1038/s41467-020-15195-y, 2020.

O'Gorman, P. A.: Contrasting responses of mean and extreme snowfall to climate change, Nature, 512, 416–418, https://doi.org/10.1038/nature13625, 2014.

Overland, J. E. and Wang, M.: Impact of the winter polar vortex on greater North America, Intl Journal of Climatology, 39, 5815–5821, https://doi.org/10.1002/joc.6174, 2019.

Pfleiderer, P., Schleussner, C.-F., Geiger, T., and Kretschmer, M.: Robust predictors for seasonal Atlantic hurricane activity identified with causal effect networks, Weather Clim. Dynam., 1, 313–324, https://doi.org/10.5194/wcd-1-313-2020, 2020.

Preece, J. R., Mote, T. L., Cohen, J., Wachowicz, L. J., Knox, J. A., Tedesco, M., and Kooperman, G. J.: Summer atmospheric circulation over Greenland in response to Arctic amplification and diminished spring snow cover, Nat Commun, 14, 3759, https://doi.org/10.1038/s41467-023-39466-6, 2023.

Previdi, M., Smith, K. L., and Polvani, L. M.: Arctic amplification of climate change: a review of underlying mechanisms, Environ. Res. Lett., 16, 093003, https://doi.org/10.1088/1748-9326/ac1c29, 2021.

Quante, L., Willner, S. N., Middelanis, R., and Levermann, A.: Regions of intensification of extreme snowfall under future warming, Sci Rep, 11, 16621, https://doi.org/10.1038/s41598-021-95979-4, 2021.

Runge, J.: Causal network reconstruction from time series: From theoretical assumptions to practical estimation, Chaos, 28, 075310, https://doi.org/10.1063/1.5025050, 2018.

Runge, J., Nowack, P., Kretschmer, M., Flaxman, S., and Sejdinovic, D.: Detecting and quantifying causal associations in large nonlinear time series datasets, Sci. Adv., 5, eaau4996, https://doi.org/10.1126/sciadv.aau4996, 2019a.

Runge, J., Bathiany, S., Bollt, E., Camps-Valls, G., Coumou, D., Deyle, E., Glymour, C., Kretschmer, M., Mahecha, M. D., Muñoz-Marí, J., van Nes, E. H., Peters, J., Quax, R., Reichstein, M., Scheffer, M., Schölkopf, B., Spirtes, P., Sugihara, G., Sun, J., Zhang, K., and Zscheischler, J.: Inferring causation from time series in Earth system sciences, Nat Commun, 10, 2553, https://doi.org/10.1038/s41467-019-10105-3, 2019b.

Sasgen, I., Wouters, B., Gardner, A. S., King, M. D., Tedesco, M., Landerer, F. W., Dahle, C., Save, H., and Fettweis, X.: Return to rapid ice loss in Greenland and record loss in 2019 detected by the GRACE-FO satellites, Commun Earth Environ, 1, 8, https://doi.org/10.1038/s43247-020-0010-1, 2020.

903 Scaife, A.A., Smith, D. A signal-to-noise paradox in climate science. npj Clim Atmos Sci 1, 28 (2018).
904 https://doi.org/10.1038/s41612-018-0038-4

905 Scherrer, S. C., Croci-Maspoli, M., Schwierz, C., and Appenzeller, C.: Two-dimensional indices of atmospheric blocking and
906 their statistical relationship with winter climate patterns in the Euro-Atlantic region, Int. J. Climatol., 26, 233–249,
907 https://doi.org/10.1002/joc.1250, 2006.

908 Screen, J. A., Deser, C., Smith, D. M., Zhang, X., Blackport, R., Kushner, P. J., Oudar, T., McCusker, K. E., and Sun, L.:
909 Consistency and discrepancy in the atmospheric response to Arctic sea-ice loss across climate models, Nature Geosci, 11, 155–
910 163, https://doi.org/10.1038/s41561-018-0059-y, 2018.

911 Serreze, M. C., Barrett, A. P., Stroeve, J. C., Kindig, D. N., and Holland, M. M.: The emergence of surface-based Arctic
912 amplification, The Cryosphere, 2009.

913 Shang, Y., Liu, P., and Wu, S.: Responses of the Pacific and Atlantic decadal variabilities under global warming by using
914 CMIP6 models, Ocean Dynamics, 74, 67–75, https://doi.org/10.1007/s10236-023-01590-8, 2024.

915 Shepherd, Andrew, Ivins, Erik, Rignot, Eric, Smith, Ben, van den Broeke, Michiel, Velicogna, Isabella, Whitehouse, Pippa,
916 Briggs, Kate, Joughin, Ian, Krinner, Gerhard, Nowicki, Sophie, Payne, Antony, Scambos, Ted, Schlegel, Nicole, A, Geruo,
917 Agosta, Cécile, Ahlstrøm, Andreas, Babonis, Greg, Barletta, Valentina, Bjørk, Anders, Blazquez, Alejandro, Bonin, Jennifer,
918 Colgan, William, Csatho, Beata, Cullather, Richard, Engdahl, Marcus, Felikson, Denis, Fettweis, Xavier, Forsberg, René,
919 Gallee, Hubert, Gardner, Alex, Gilbert, Lin, Gourmelen, Noel, Groh, Andreas, Gunter, Brian, Hanna, Edward, Harig,
920 Christopher, Helm, Veit, Hogg, Anna, Horvath, Alexander, Horwath, Martin, Khan, Shfaqat, Kjeldsen, Kristian, Konrad,
921 Hannes, Langen, Peter, Lecavalier, Benoit, Loomis, Bryant, Luthcke, Scott, McMillan, Malcolm, Melini, Daniele, Mernild,
922 Sebastian, Mohajerani, Yara, Moore, Philip, Mottram, Ruth, Mouginot, Jeremie, Moyano, Gorka, Muir, Alan, Nagler, Thomas,
923 Nield, Grace, Nilsson, Johan, Noël, Brice, Otosaka, Inès, Pattle, Mark, Peltier, W, Pie, Nadège, Rietbroek, Roelof, Rott,
924 Helmut, Sørensen, Louise Sandberg, Sasgen, Ingo, Save, Himanshu, Scheuchl, Bernd, Schrama, Ernst, Schröder, Ludwig, Seo,
925 Ki-Weon, Simonsen, Sebastian, Slater, Thomas, Spada, Giorgio, Sutterley, Tyler, Talpe, Matthieu, Tarasov, Lev, van de Berg,
926 Willem Jan, van der Wal, Wouter, van Wessem, Melchior, Vishwakarma, Bramha Dutt, Wagner, Thomas, Wiese, David,
927 Wilton, David, Wouters, Bert, and Wuite, Jan: Antarctic and Greenland Ice Sheet mass balance 1992-2020 for IPCC AR6
928 (1.0), https://doi.org/10.5285/77B64C55-7166-4A06-9DEF-2E400398E452, 2021.

929 Shu, Q., Wang, Q., Årthun, M., Wang, S., Song, Z., Zhang, M., and Qiao, F.: Arctic Ocean Amplification in a warming climate
930 in CMIP6 models, Sci. Adv., 8, eabn9755, https://doi.org/10.1126/sciadv.abn9755, 2022.

931 Tedesco, M. and Fettweis, X.: Unprecedented atmospheric conditions (1948–2019) drive the 2019 exceptional melting season
932 over the Greenland ice sheet, The Cryosphere, 14, 1209–1223, https://doi.org/10.5194/tc-14-1209-2020, 2020.

933 Tedesco, M., Fettweis, X., van den Broeke, M. R., van de Wal, R. S. W., Smeets, C. J. P. P., van de Berg, W. J., Serreze, M.
934 C., and Box, J. E.: The role of albedo and accumulation in the 2010 melting record in Greenland, Environ. Res. Lett., 6, 014005,
935 https://doi.org/10.1088/1748-9326/6/1/014005, 2011.

936 Tian, Y., Giaquinto, D., Di Capua, G. et al.: Historical changes in the Causal Effect Networks of compound hot and dry
937 extremes in central Europe. Commun Earth Environ 5, 764 (2024). https://doi.org/10.1038/s43247-024-01934-2

938 Tibaldi, S. and Molteni, F.: On the operational predictability of blocking, Tellus A, 42, 343–365,
939 https://doi.org/10.1034/j.1600-0870.1990.t01-2-00003.x, 1990.

940 Tyrlis E, Bader J, Manzini E, Matei D. Reconciling different methods of high-latitude blocking detection. Q J R Meteorol Soc.
941 2021; 147: 1070–1096. https://doi.org/10.1002/qj.39

942 Topál, D., Ding, Q., Ballinger, T. J., Hanna, E., Fettweis, X., Li, Z., and Pieczka, I.: Discrepancies between observations and
943 climate models of large-scale wind-driven Greenland melt influence sea-level rise projections, Nat Commun, 13, 6833,
944 https://doi.org/10.1038/s41467-022-34414-2, 2022.

945 Wachowicz, L. J., Preece, J. R., Mote, T. L., Barrett, B. S., and Henderson, G. R.: Historical trends of seasonal Greenland
946 blocking under different blocking metrics, Intl Journal of Climatology, 41, https://doi.org/10.1002/joc.6923, 2020.

947 Wang, H. and Luo, D.: North Atlantic Footprint of Summer Greenland Ice Sheet Melting on Interannual to Interdecadal Time
948 Scales: A Greenland Blocking Perspective, Journal of Climate, 35, 1939–1961, https://doi.org/10.1175/JCLI-D-21-0382.1,
949 2022.

950 Wang, S. S., Huang, W., and Yoon, J.: The North American winter 'dipole' and extremes activity: a CMIP5 assessment,
951 Atmospheric Science Letters, 16, 338–345, https://doi.org/10.1002/asl2.565, 2015.

952 Woollings, T. and Hoskins, B.: Simultaneous Atlantic–Pacific blocking and the Northern Annular Mode, Quart J Royal
953 Meteoro Soc, 134, 1635–1646, https://doi.org/10.1002/qj.310, 2008.

954 Woollings, T., Barriopedro, D., Methven, J., Son, S.-W., Martius, O., Harvey, B., Sillmann, J., Lupo, A. R., and Seneviratne,
955 S.: Blocking and its Response to Climate Change, Curr Clim Change Rep, 4, 287–300, https://doi.org/10.1007/s40641-018-
956 0108-z, 2018.

957 Ye, K. and Jung, T.: How Strong Is Influence of the Tropics and Midlatitudes on the Arctic Atmospheric Circulation and
958 Climate Change?, Geophysical Research Letters, 46, 4942–4952, https://doi.org/10.1029/2019GL082391, 2019.

959 Zhang, B., Liu, L., Khan, S. A., van Dam, T., Bjørk, A. A., Peings, Y., Zhang, E., Bevis, M., Yao, Y., and Noël, B.: Geodetic
960 and model data reveal different spatio-temporal patterns of transient mass changes over Greenland from 2007 to 2017, Earth
961 and Planetary Science Letters, 515, 154–163, https://doi.org/10.1016/j.epsl.2019.03.028, 2019.

962 Zhu, Z., Lu, R., Yu, B., Li, T., and Yeh, S.-W.: A moderator of tropical impacts on climate in Canadian Arctic Archipelago
963 during boreal summer, Nat Commun, 15, 8644, https://doi.org/10.1038/s41467-024-53056-0, 2024